Electronic Supplementary Material (ESI) for Energy & Environmental Science.
This journal is © The Royal Society of Chemistry 2024

Supplementary Information

1. Experimental Section

Materials

BTP-eC9 and PNDIT-F3N were purchased from Organtec. Ltd. Chloroform was distilled from CaH_2 prior to use. Other reagents used were purchased from commercial sources and used as received. Compound (**I**) 12,13-bis(2-butyloctyl)-3,9-diundecyl-12,13-dihydro-[1,2,5]thiadiazolo[3,4-e]thieno[2'',3'':4',5']thieno[2',3':4,5]pyrrolo[3,2-g]thieno[2',3':4,5]thieno[3,2-b]indole-2,10-dicarbaldehyde was synthesized according to the procedures outlined in the literatures.[1, 2] The synthetic route of Se-Giant was shown in **Scheme S1**. ^{1}HNMR spectra was measured on Bruker AVANCE 600 MHz and JEOL JNM-ECZ 400MHz spectrometer with *d* chloroform as the solvent. The chemical shifts were reported as δ value (ppm) relative to an internal tetramethylsilane (TMS) standard. Mass spectra (MALDI-TOF-MS) were determined using AB SCIEX 5800 Mass Spectrometer.

Synthesis of Se-Giant

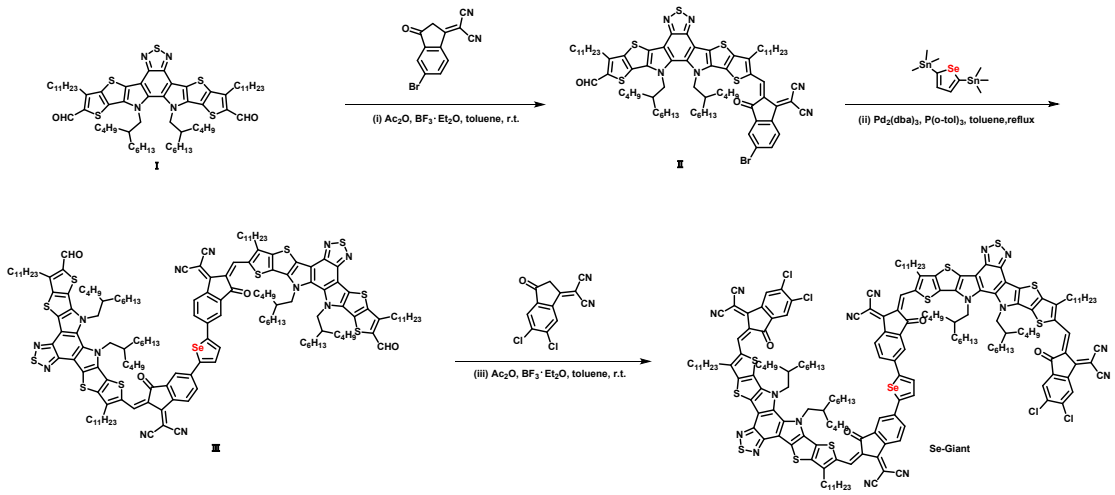

Scheme S1. The overall synthetic route to Se-Giant. Reagents and conditions: (i) 2-(5-bromo-3-oxo-2,3-dihydro-1*H*-inden-1-ylidene)malononitrile, Ac_2O, $BF_3{\cdot}Et_2O$, toluene, room temperature; (ii) 2,5-bis(trimethylstannyl)selenophene, $Pd_2(dba)_3$, P(*o*-

tol)$_3$, toluene, reflux; (iii) 2-(5,6-dichloro-3-oxo-2,3-dihydro-1*H*-inden-1-ylidene)malononitrile, Ac_2O, $BF_3{\cdot}Et_2O$, toluene, room temperature.

Synthesis of compound II. Under the protection of argon, compound **I** (500 mg, 0.439 mmol, 1.0 eq.), 2-(5-bromo-3-oxo-2,3-dihydro-1*H*-inden-1-ylidene)malononitrile (180mg, 0.658 mmol, 1.5 eq.), acetic anhydride (0.5 mL) and dry toluene (15 mL) was added to 50 mL two-necked round bottom flask. $BF_3{\cdot}Et_2O$ (0.5 mL) was added dropwise to the mixture solution at 0 ℃. Then the mixture was stirred at room temperature. After 30 mins, the reaction mixture was precipitated in methanol (100 mL). The precipitate was purified by flash silica gel chromatography with petroleum ether/ dichloromethane (v/v=1/1) as eluent to afford the compound II (260 mg, 42%).

^{1}H NMR (600 MHz, Chloroform-*d*) δ 10.16 (s, 1H), 9.17 (s, 1H), 8.55 (d, *J* = 8.3 Hz, 1H), 8.02 (d, *J* = 1.9 Hz, 1H), 7.84 (dd, *J* = 8.4, 2.0 Hz, 1H), 4.74 (d, *J* = 7.7 Hz, 2H), 4.66 (d, *J* = 7.8 Hz, 2H), 3.21 (td, *J* = 8.0, 2.7 Hz, 4H), 2.09 (p, *J* = 6.3 Hz, 2H), 1.96 - 1.85 (m, 4H), 1.50 (dt, *J* = 15.7, 7.9 Hz, 4H), 1.41 - 1.35 (m, 4H), 1.28 - 1.25 (m, 12H), 1.17-1.10 (m, 12H), 1.06 - 0.92 (m, 32H), 0.87 - 0.78 (m, 18H).

Synthesis of compound III. The compound II (260 mg, 0.186 mmol, 3.0 eq.), 2,5-bis(trimethylstannyl)selenophene (28.4 mg, 0.062 mmol, 1.0 eq.), $Pd_2(dba)_3$ (2.8 mg, 3.0 μmol, 0.05 eq.), and P(*o*-tol)$_3$ (9.1 mg, 0.03 mmol, 0.5 eq.) were added into 100 mL two-necked round bottom flask and dissolved in toluene (30 mL). The flask was purged with nitrogen and sealed under nitrogen flow. The resulting mixture was stirred and heated to reflux overnight. After cooling to room temperature, the mixture solution was poured into methanol (100 mL). The precipitate was purified by silica gel column chromatography with petroleum ether/chloroform (v/v=1/1) as eluent to obtain compound III (79 mg, 79%).

^{1}H NMR (600 MHz, Chloroform-*d*) δ 10.17 (s, 2H), 9.15 (s, 2H), 8.74 (d, *J* = 8.1 Hz, 2H), 8.05 (s, 2H), 7.91 (dd, *J* = 8.0, 1.9 Hz, 2H), 7.79 (s, 2H), 4.84 – 4.73 (m, 4H), 4.71 - 4.65 (m, 4H), 3.22 (t, *J* = 7.9 Hz, 8H), 2.17 (s, 4H), 2.11 (d, *J* = 17.0 Hz, 4H), 1.94 (p,

J = 7.8 Hz, 4H), 1.90 - 1.85 (m, 4H), 1.53 - 1.34 (m, 18H), 1.33 - 1.21 (m, 60H), 1.11 - 0.93 (m, 34H), 0.92 - 0.80 (m, 24H), 0.74 - 0.62 (m, 24H).

Synthesis of compound Se-Giant. Under the protection of nitrogen, compound III (79.0 mg, 0.028 mmol, 1.0 eq.), 2-(5,6-dichloro-3-oxo-2,3-dihydro-1*H*-inden-1-ylidene)malononitrile (30.1 mg, 0.114 mmol, 4.0 eq.), acetic anhydride (0.1 mL) and dry toluene (5 mL) was added to 25 mL two-necked round bottom flask. Then $BF_3 \cdot Et_2O$ (0.5 mL) was added dropwise to the mixture solution at room temperature. After 30 mins, the reaction mixture was precipitated in methanol (100 mL). The precipitate was purified by column chromatography on silica gel with petroleum ether/chloroform (v/v=1/2) as eluent to afford Se-Giant (35 mg, 38%).

^{1}H NMR (600 MHz, Chloroform-*d*, room temperature) δ 9.21 (s, 2H), 8.93 (s, 2H), 8.77 (s, 4H), 8.07 (d, *J* = 8.1 Hz, 2H), 8.01 (s, 2H), 7.84 (s, 2H), 7.59 (s, 2H), 4.90 - 4.77 (m, 8H), 3.27 (s, 4H), 3.12 (s, 4H), 2.24 (s, 2H), 2.17 (s, 2H), 2.05 - 1.98 (m, 4H), 1.92 (s, 4H), 1.82 (s, 4H), 1.67 - 1.47 (m, 64H), 1.43 - 1.22 (m, 56H), 0.91 - 0.59 (m, 40H).

^{1}H NMR (400 MHz, Chloroform-*d*, 323.15K) δ 9.18 (s, 2H), 8.96 (s, 2H), 8.74 (d, *J* = 9.6 Hz, 4H), 8.04 - 7.96 (m, 4H), 7.80 (s, 2H), 7.63 (s, 2H), 4.85 (s, 8H), 3.26 (t, *J* = 7.9 Hz, 4H), 3.13 (t, *J* = 7.9 Hz, 4H), 2.26 - 2.15 (m, 4H), 1.95 - 1.89 (m, 4H), 1.87 - 1.80 (m, 4H), 1.32 - 1.24 (m, 68H), 1.14 - 1.03 (m, 24H), 1.03 - 0.94 (m, 21H), 0.91 - 0.81 (m, 27H), 0.76 - 0.61 (m, 24H).

MALDI-TOF MS (m/z): calcd for $C_{184}H_{208}Cl_4N_{16}O_4S_{10}Se$: 3248.1695 Found: 3248.5773.

***Nuclear magnetic resonance (NMR)*:** ^{1}H NMR spectrum was recorded on Bruker AVANCE NEO 600 MHz spectrometer with *d* chloroform as the solvent. The chemical shifts were reported as δ value (ppm) relative to an internal tetramethylsilane (TMS) standard.

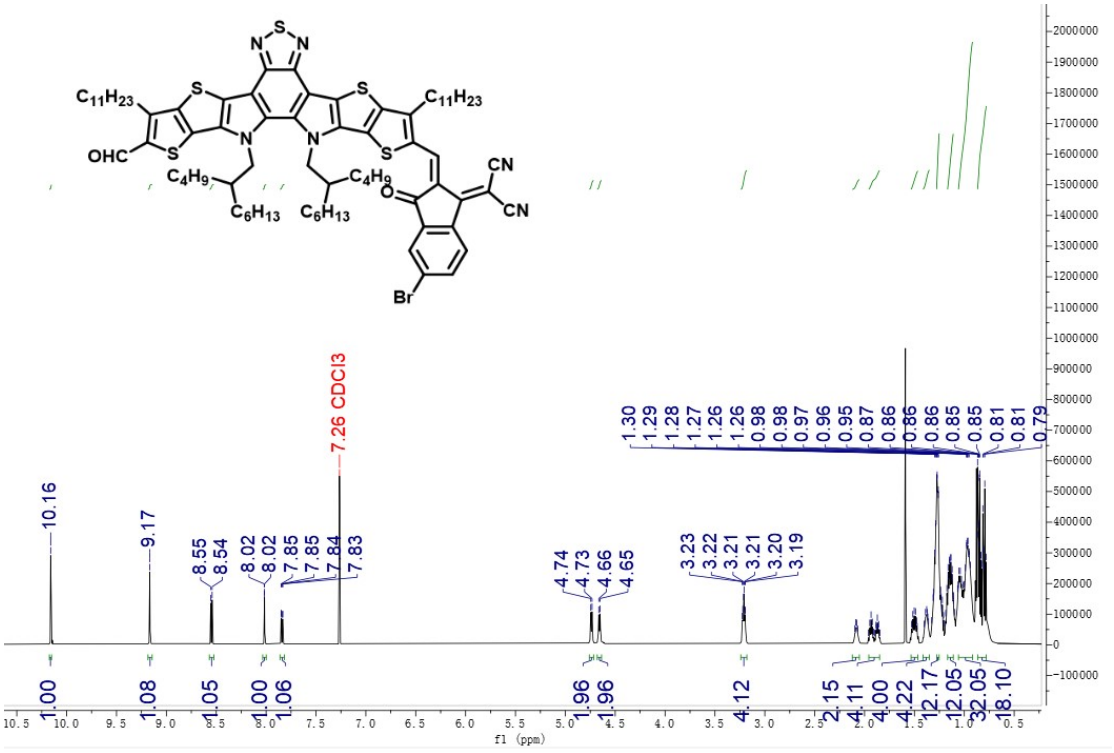

Figure S1. ^{1}H NMR of compound II.

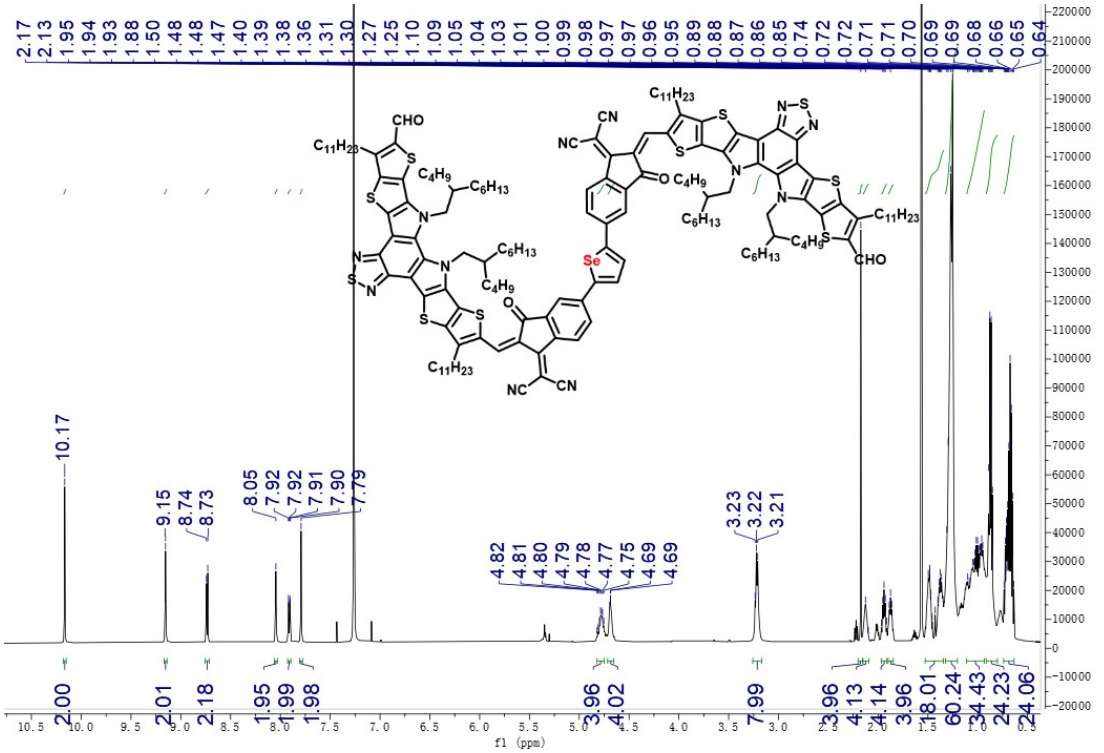

Figure S2. [1]H NMR of compound III.

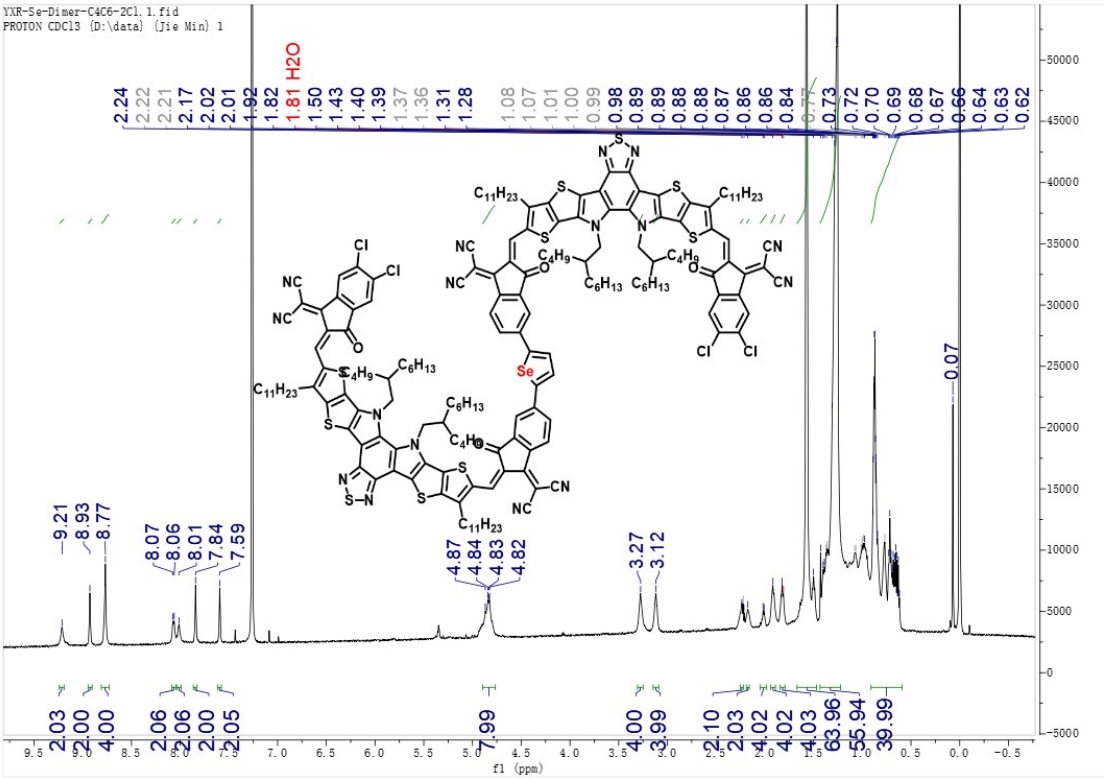

Figure S3. [1]H-NMR spectrum of giant molecule acceptor Se-Giant (600M, r.t.).

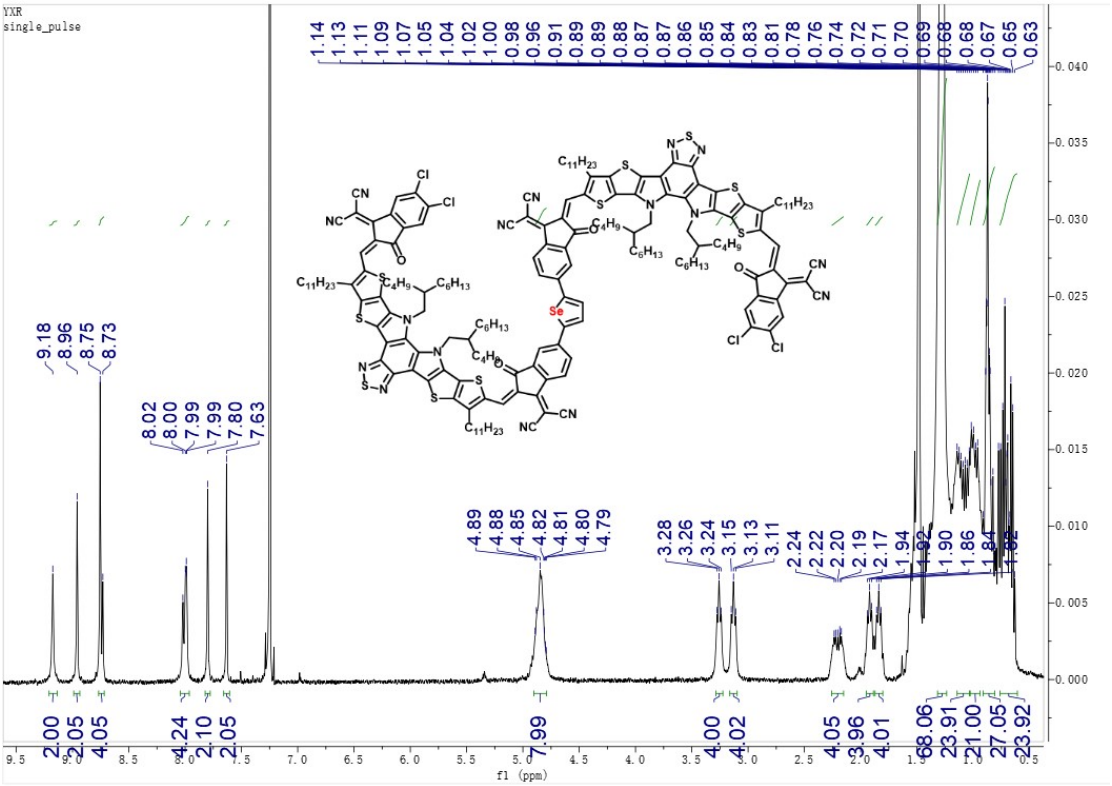

Figure S4. [1]H-NMR spectrum of giant molecule acceptor Se-Giant (400M, 323.15K).

Matrix-assisted laser desorption/ionization time-of-flight (MALDI-TOF) Mass: MALDI-TOF mass spectra was determined using AB SCIEX 5800 Mass Spectrometer.

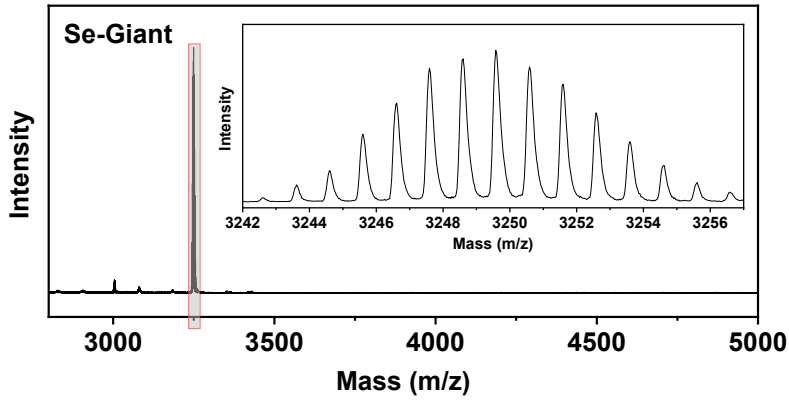

Figure S5. Mass spectrum of giant molecule acceptor Se-Giant.

***Electrochemical characterizations*:** Electrochemical properties were studied by cyclic voltammetry (CV), which was performed on a CS350H electrochemical workstation with a three-electrode system in a 0.1 M Bu_4NPF_6 acetonitrile solution at a scan rate of 100 mV s^{-1}. Glassy carbon disc coated with sample film was used as the working electrode. A Pt wire was used as the counter electrode and Ag/AgCl was used as the reference electrode. The HOMO/LUMO energy levels (E_{HOMO}/E_{LUMO}) can be calculated from onset oxidation/reduction potentials (ϕox/ϕred) in the cyclic voltammograms according to the equations of E_{HOMO}/E_{LUMO} =-e(ϕ_{OX}/ ϕ_{Red} +4.8-ϕ_{Fe/Fe^+}) (eV) (eV), where ϕ_{Fe/Fc^+} is the redox potential of ferrocene/ferrocenium (Fe/Fc^+) couple in the electrochemical measurement system, and the energy level of Fe/Fc^+ was taken as 4.8 eV below vacuum.

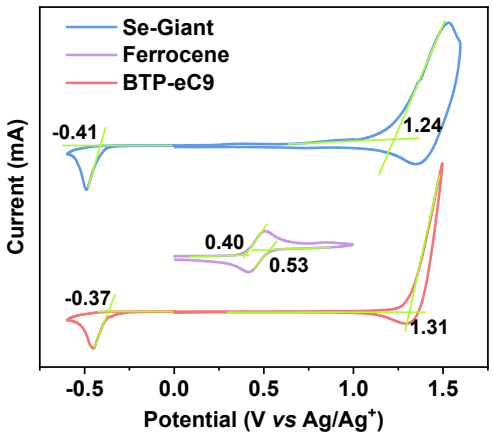

Figure S6. Cyclic voltammetry curves of Ferrocene, Se-Giant, and BTP-eC9 in acetonitrile solution with 0.1 M n-Bu_4PF_6 as the supporting electrolyte, at with a scanning rate of 100 mV s^{-1}.

Optical measurements and simulations: Ultraviolet-visible near-infrared (UV-vis-NIR) absorption spectra were recorded with a Perkin-Elmer Lambda 365 UV-Vis spectrophotometer from 300 nm to 1100 nm.

Table S1. Optical and electrochemical properties of MPhS-C2, Se-Giant and BTP-eC9.

Materials	$\lambda_{max,sol}$ (nm)	$\lambda_{max,film}$ (nm)	$\lambda_{onset,film}$ (nm)	E_g[a] (eV)	LUMO/HOMO[b] (eV)
MPhS-C2	--	585	705	1.76	-3.45/-5.35
Se-Giant	743	797	891	1.39	-3.92/-5.57
BTP-eC9	747	833	917	1.35	-3.97/-5.65

[a)]Calculated from the absorption onset of the films. [b)]Estimated from the reduction/oxidation onset of the CV curves.

***Differential scanning calorimetry (DSC) measurements*:** DSC (DSC Q2000 V24.11 Build 124) curves were performed at a heating and cooling rate of 10°C min^{-1} under nitrogen atmosphere.

***Space charge limited current (SCLC) measurements*:** Single carrier devices were fabricated and the dark current-voltage characteristics measured and analyzed in the space charge limited (SCL) regime following the references. The structure of hole only devices was Glass/ITO/PEDOT:PSS/Active layer/MoO_3 (10nm)/Ag (100 nm). For the electron only devices, the structure was Glass/ITO/ZnO/Active layer/PNDIT-F3N/Ag (100 nm), where the Ag were evaporated. The *J-V* characteristics of both hole-only and electron-only diodes can be excellently fit to the Mott-Gurney relation for space charge limited current: $J_{SCL} = \frac{9}{8}\varepsilon_0\varepsilon_r\mu\frac{V_{in}^2}{L^3}exp\left(\frac{0.89 \times \beta}{\sqrt{L}}\sqrt{V_{in}}\right)$, Where J_{SCL} is the current density, ε_0 is the permittivity of free-space, ε_r is the relative dielectric constant of the active layer, μ is the charge carrier mobility, β is the field activation factor, L is the thickness of the device and V_{in} is the voltage dropped across the sample.

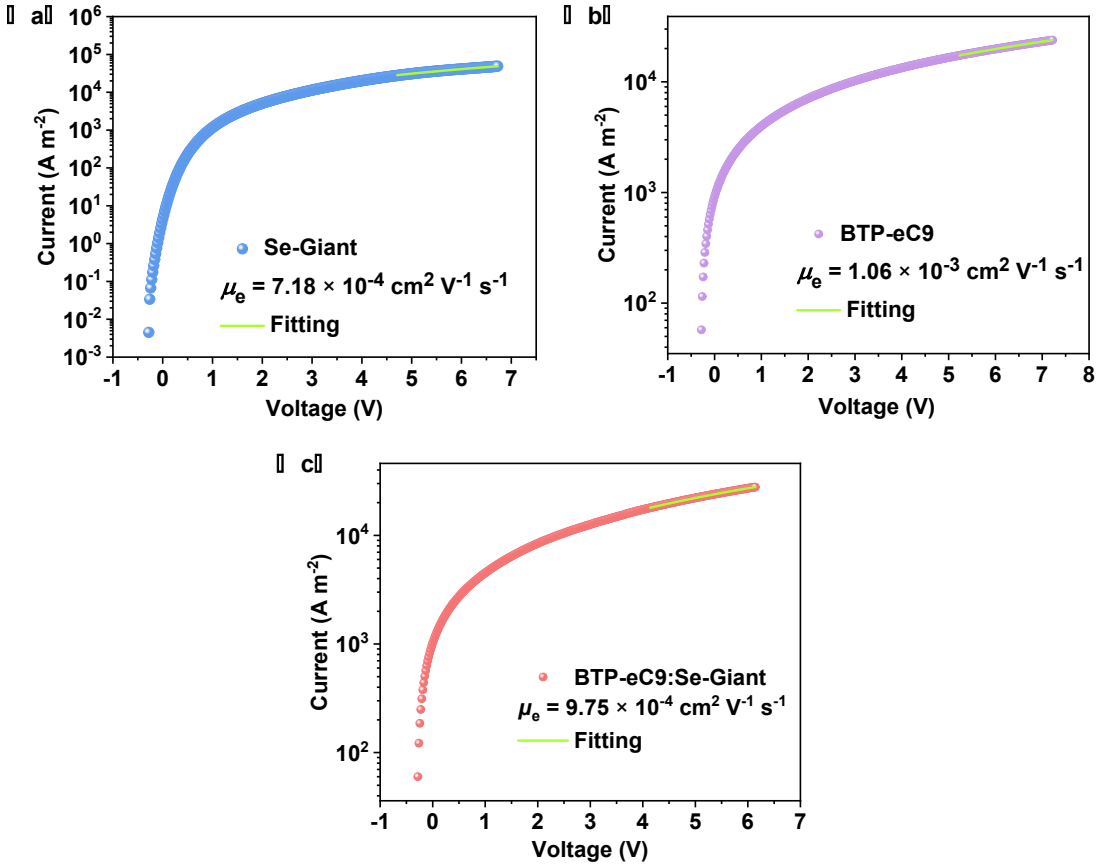

Figure S7. The dark *J-V* characteristics of pristine (a) Se-Giant, (b) BTP-eC9, and (c) BTP-eC9:Se-Giant (0.8:0.2, wt%) films-based electron-only devices. The solid lines represent the best fitting using the SCLC model.

***Grazing incidence wide angle X-ray scattering (GIWAXS) characterization*:** GIWAXS measurements with Kα X-ray of Cu source (8.05 keV, 1.54 Å) and a Pilatus3R 300 K detector were conducted at a Xeuss 2.0 WAXS laboratory beamline. Samples were prepared by spin coating identical chloroform blend solutions as those used in devices on Si substrates. The grazing incident angle was 0.18°.

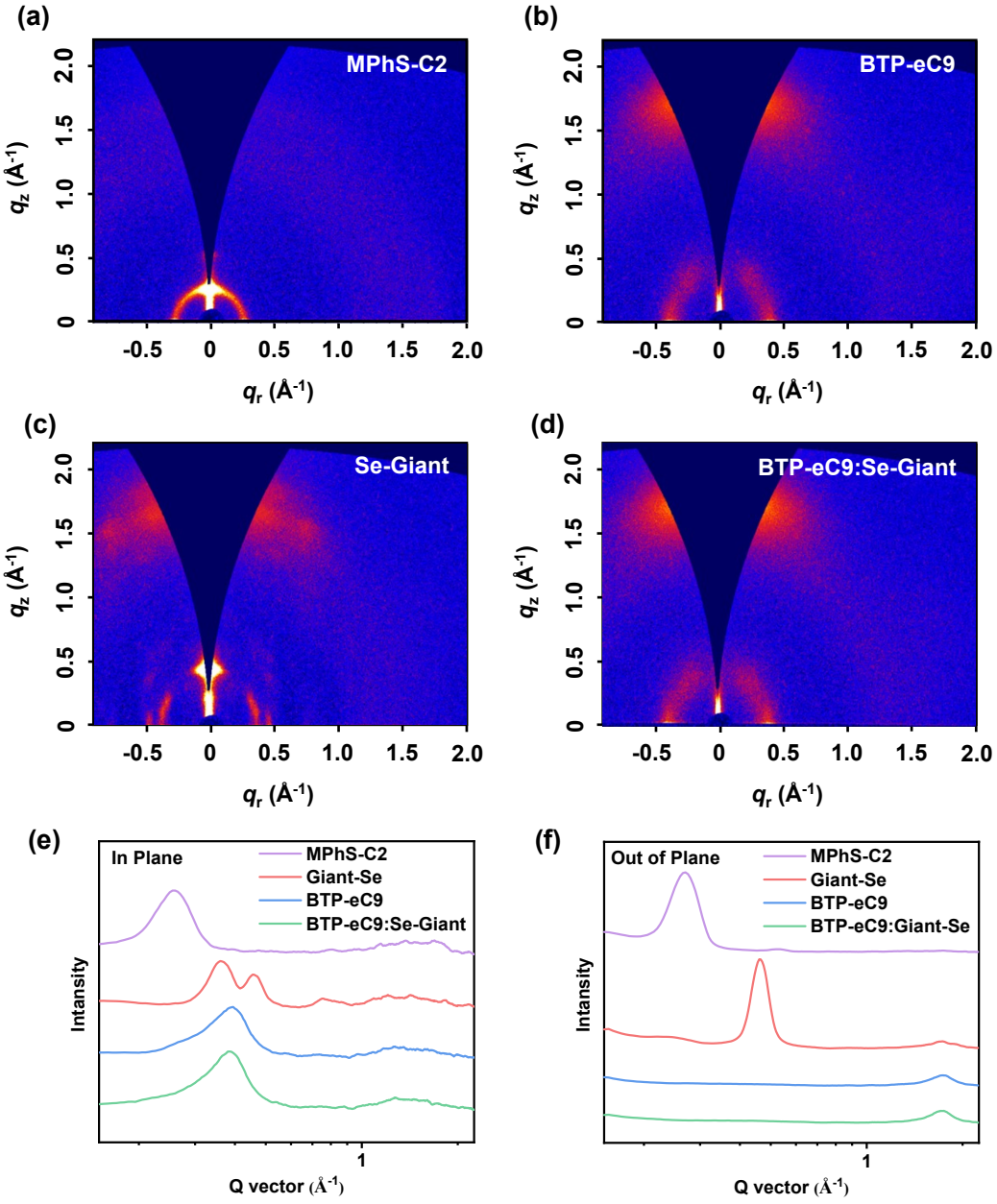

Figure S8. 2D GIWAXS patterns of (a) MPhS-C2, (b) BTP-eC9, (c) Se-Giant (d) BTP-eC9:Se-Giant (0.8:0.2, wt%) films; Scattering profiles of in-plane (IP) (e) and out-of-plane (OOP) (f) for the corresponding films.

Table S2. Investigations of the morphology parameters extracted from the GIWAXS measurements of the MPhS-C2, Se-Giant, BTP-eC9 and BTP-eC9:Se-Giant (1:0.2, wt%) films.

Neat films	In-plane (100)		Out-of-plane (010)			
	q (Å^{-1})	d-spacing (Å)	*q* (Å^{-1})	d-spacing (Å)	FWHM (Å^{-1})	Coherence length (Å)
MPhS-C2	0.26	24.17	/	/	/	/
Se-Giant	0.36	17.45	1.73	3.63	0.39	16.07
BTP-eC9	0.40	15.90	1.74	3.62	0.31	20.06
BTP-eC9:Se-Giant	0.38	16.32	1.74	3.60	0.32	19.64

***Contact angle measurements and surface energy calculation*:** The contact angles of two acceptors (BTP-eC9 and Se-Giant), donor MPhS-C2 and the blend of BTP-eC9:Se-Giant were measured using a Contact Angle Analyzer. The contact angles of wo different solvents (water and ethylene glycol (EG)) on the neat films were used to calculate the surface tension of each film by the Wu model.

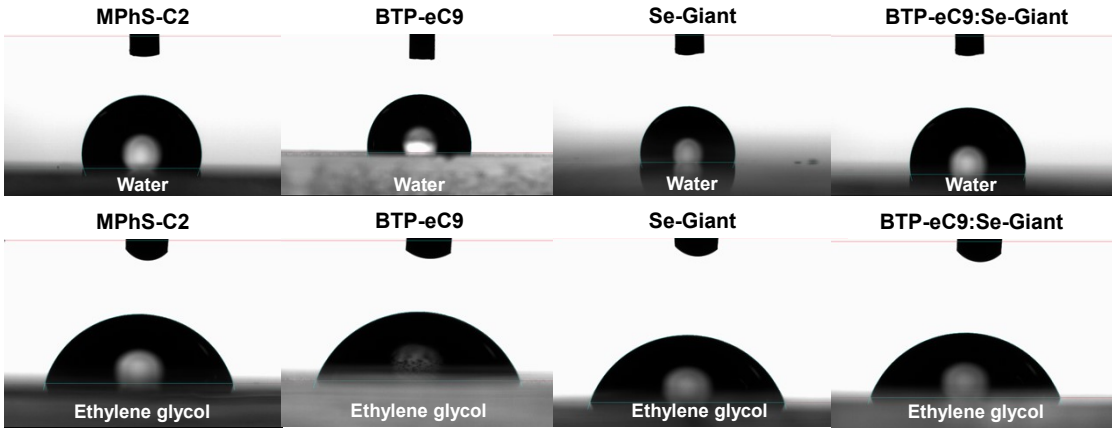

Figure S9. Photographs of water and ethylene glycol droplets on the top surfaces of MPhS-C2, BTP-eC9, Se-Giant and BTP-eC9:Se-Giant. The contact angle measurement is conducted at the center of the substrates, avoiding the edges of the ITO anodes. The contact angles of two different solvents on the neat films were used to calculate the surface tension of each film by the Owens-Wendt method.[3]

Table S3. Investigations of the contact angles, surface energy, wetting coefficient and Flory–Huggins interaction parameter (χ) values of MPhS-C2, BTP-eC9 and BTP-eC9:Se-Giant.

Materials	Contact angles (°)		Surface energy (mN m^{-1})	Relative χ values[a]	
	Water	Ethylene glycol		(With MPhS-C2)	(With BTP-eC9)
MPhS-C2	104.9 (104.9±0.06)	74.3 (74.3±0.03)	55.25 (55.25±0.08)	/	/
BTP-eC9	97.9 (97.9±0.07)	68.5 (68.5±0.04)	45.32 (45.32±0.09)	0.25K	/
Se-Giant	101.2 (101.2±0.05)	71.3 (71.3±0.06)	48.28 (48.28±0.08)	0.08 K	0.05 K
BTP-eC9:Se-Giant	99.7 (99.7±0.04)	70.3 (70.3±0.05)	46.00 (46.00±0.06)	0.20 K	/

[a]The Flory-Huggins interaction parameter χ_{D-A} is derived using the empirical equation[4]: $\chi_{D-A} = K(\sqrt{\gamma_D} - \sqrt{\gamma_A})^2$, where K is a positive constant; γ_D and γ_A are surface

tensions obtained from contact angle measurements, χ is the Flory-Huggins interaction parameter.

Device Fabrication and Testing

Solar cells were fabricated in a conventional device configuration of ITO/PEDOT:PSS (40nm)/MPhS-C2:acceptors/PNDIT-F3N/Ag. Pre-patterned ITO-coated glass substrates (purchased from South China Science & Technology Company Limited) washed with methylbenzene, deionized water, acetone and isopropyl alcohol in an ultrasonic bath for 15 min each. After blow-dried by high-purity nitrogen, All ITO substrates are cleaned in ultraviolet ozone cleaning system for 15 min. Subsequently, a thin layer of PEDOT: PSS (Xi'an Yuri Solar Co., Ltd.) was deposited through spin-coating at 4500 rpm for 30s on pre-cleaned ITO-coated glass from a PEDOT: PSS aqueous solution and annealed at 150 °C for 15 min in atmospheric air. The MPhS-C2: acceptor blends (1.7:1 weight ratio) were dissolved in chloroform solution with 0.25% additive of 1,8-diiodooctane (DIO). The total concentration of blend solutions was 18 mg mL^{-1} for all blends and stirred at 45 °C for 3 hours. The blend solution was spin-coated at 3200 rpm for 30 s. Then the device thermal annealed at 115 °C for 7 min, and solvent (CF) annealed for 60 seconds. The thickness optimal active layer measured by a Bruker Dektak XT stylus profilometer was about 110 nm. Then methanol solution of PNDIT-F3N at a concentration of 0.5 mg mL^{-1} was spin-coated onto the active layer at 4000 rpm for 30s. Finally, the top argentum electrode of 100 nm thickness was thermally evaporated through a mask onto the cathode buffer layer under a vacuum of ~5×10^{-6} mbar. The typical active area of the investigated devices was 0.048 cm^2 and the area of a non-refractive mask used was 0.0289 cm^2. The current-voltage characteristics of the solar cells were measured by a Keithley 2400 source meter unit under AM1.5G (100 mW cm^{-2}) irradiation from a solar simulator (Enlitech model SS-X160R). Solar simulator illumination intensity was determined at 100 mW cm^{-2} using a monocrystalline silicon reference cell with a KG5 filter. Short circuit currents under AM1.5G (100 mW cm^{-2}) conditions were estimated from the spectral response and convolution with the solar spectrum. The forward scan was adopted to test the *J-V*

curves, and the scan step is 0.02 V and the delay time is 1 ms. The scan mode is sweep.

External quantum efficiency (EQE) measurements: The external quantum efficiency was measured by a Solar Cell Spectral Response Measurement System QE-R3011(Enli Technology Co., Ltd.).

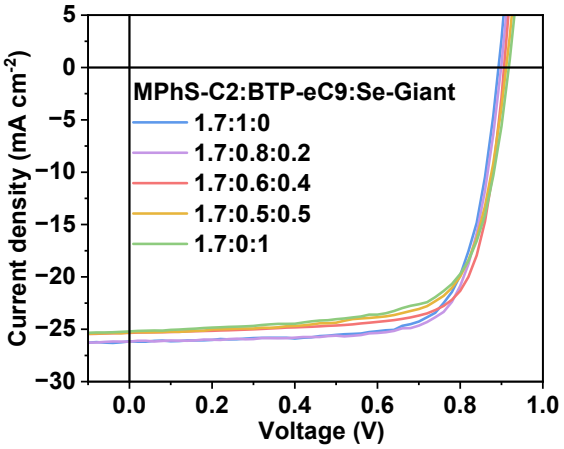

Figure S10. *J-V* characteristics for devices based on MPhS-C2:BTP-eC9:Se-Giant, with different Se-Giant ratio in acceptor, measured under the illumination of AM 1.5 G at 100 mW cm^{-2}.

Table S4. Summary of photovoltaic parameters of the all-SMOSCs based on MPhS-C2:BTP-eC9:Se-Giant with different Se-Giant ration, measured under the illumination of AM 1.5 G at 100 mW cm^{-2}.

MPhS-C2:BTP-eC9:Se-Giant	V_{OC} (V)	J_{SC} (mA/cm^2)	FF (%)	PCE (%)
1.7:1:0	0.892	26.16	73.66	17.19 (16.98±0.10)
1.7:0.8:0.2	0.903	26.34	76.33	18.16 (18.01±0.12)
1.7:0.6:0.4	0.907	25.32	75.39	17.31 (17.12±0.10)
1.7:0.5:0.5	0.911	25.30	71.91	16.58 (16.22±0.15)
1.7:0:1	0.918	25.21	70.34	16.28 (16.02±0.12)

[a)]The average PCE values with standard deviations were obtained from 10 independent cells.

Table S5. Summary of E_{loss}, PCE and the corresponding photovoltaic parameters of all-SMOSCs

Donor	Acceptor	V_{OC} (V)	J_{SC} (mA cm^{-2})	FF (%)	PCE (%)	E_{loss} (eV)	Reference
H11	IDIC	0.977	15.21	65.46	9.73	0.673	5, 6
H12	IDIC	0.955	10.51	54.89	5.51	0.695	
BTID-2F	IDIC	0.9	13.98	65.20	8.23	0.75	5, 7
NDT-3T-R4	IDIC-4F	0.76	17.02	71.4	9.2	0.86	5, 8
NDT-3T-R6	IDIC-4F	0.78	18.89	72.8	10.7	0.84	
ZnP2BT-RH	$PC_{71}BM$	0.845	17.66	67.15	10.02	0.56	9
ZnP-TBO	6TIC	0.80	20.44	73.87	12.08	0.57	5, 10
ZnP-TBO	6TIC	0.84	14.92	47.87	6.0	0.53	
BSFTR	Y6	0.85	23.16	69.66	13.69	0.48	11
BTR	Y6	0.85	22.25	56.4	10.67	0.53	5, 12
BTR-Cl	Y6	0.86	24.17	65.5	13.61	0.52	
ZR1	IDIC-4Cl	0.776	18.27	67.96	9.64	0.78	13
ZR1	Y6	0.861	24.34	68.44	14.34	0.54	
BDTF-CA	IDIC-4F	0.88	14.96	63.95	8.42	0.74	5, 14
BDTF-CA	IDIC	0.99	12.09	51.14	6.12	0.66	
BDTF-CA	IDIC-2F	0.94	16.69	58.07	9.11	0.65	
BSCl-C2	IDIC-4Cl	0.865	20.1	71.3	12.40	0.655	15
ZR2-C1	Y6	0.848	21.35	65.12	11.79	0.532	5, 16
ZR2-C2	Y6	0.852	23.03	65.43	12.84	0.528	
ZR2-C3	Y6	0.854	024.69	70.06	14.78	0.526	
SM1	Y6	0.805	23.59	67.0	12.72	0.575	17
SM1-F	Y6	0.866	23.25	69.9	14.07	0.514	
SM1-S	Y6	0.825	23.23	67.7	12.95	0.555	
BTEC-1F	Y6	0.87	21.21	61.35	11.33	0.51	5, 18
BTEC-2F	Y6	0.854	21.55	72.35	13.34	0.526	
BTEC-2F	Y6	0.895	14.51	51.54	6.69	0.485	
BSCl	IDIC-4Cl	0.9	7.7	33.9	2.35	0.723	9
BSCl(TA)	IDIC-4Cl	0.845	19.1	65.6	10.57	0.745	
BSCl(TA+SVA)	IDIC-4Cl	0.865	21.5	70.0	13.03	0.721	
B1	BO-4Cl	0.83	25.27	73	15.3	0.567	5, 19
BTR	BO-4Cl	0.83	18.93	72	11.3	0.567	
BT-2F	N3	0.876	19.19	48.12	8.09	0.493	20
BT-2F(CS2)	N3	0.845	24.28	75.02	15.39	0.521	
BT-2F(TA)	N3	0.829	24.51	72.15	14.66	0.529	
B1	BO-4Cl:BO-2Cl	0.84	26.05	78.0	17.0	0.57	21
FBD-S3	Y6	0.849	27.11	67.74	12.53	0.531	5, 22
TBD-S4	Y6	0.854	24.53	72.10	15.10	0.526	
C-2F	N3	0.85	24.87	69.33	14.64	0.516	23
C-F	N3	0.79	20.51	47.52	7.76	0.576	

M-PhS	BTP-eC9	0.84	25.4	75.6	16.2	0.551	24
P-PhS	BTP-eC9	0.88	21.6	62.6	11.9	0.493	
SM-CA	N3	0.838	24.33	75.62	15.41	0.528	25
SM-CA-Reh	N3	0.842	25.06	77.5	16.34	0.524	
SM-Reh	N3	0.834	25.42	69.64	14.76	0.532	
MPhS-C2	BTP-eC9	0.886	26.86	69.52	16.54	0.498	26
MPhS-C2(DIO)	BTP-eC9	0.888	26.62	72.38	17.11	0.497	
MPhS-C4	BTP-eC9	0.873	25.61	70.28	15.73	0.518	
MPhS-C6	BTP-eC9	0.840	25.49	75.6	16.2	0.545	
BP-Cl	BO-4Cl	0.8	18.47	46.36	6.85	0.597	27
BM-Cl	BO-4Cl	0.826	25.9	73.55	15.73	0.571	
ZR-C8	Y6	0.829	25.0	58.8	12.2	0.558	28
ZR-SiO	Y6	0.852	26.0	72.3	16.0	0.537	
ZR-SiO-EH	Y6	0.870	25.6	73.7	16.4	0.518	
BTR-Cl	L8-BO	0.86	23.72	73.0	15.0	0.56	29
TB	L8-BO	0.86	24.67	74.2	17.0	0.56	
TB-F	L8-BO	0.87	25.41	76.7	15.8	0.55	
SW1	Y6	0.806	25.09	63.8	12.9	0.563	30
SW2	Y6	0.835	25.10	74.0	15.51	0.528	
BSFTR	FO-EH-2Cl	0.876	22.39	80.44	15.78	0.639	31
BSFTR	FO-2Cl	0.885	22.01	78.41	15.27	0.638	
B1	L8-BO	0.858	24.57	75.03	15.82	0.569	32
B1	BO-4Cl	0.822	25.51	73.61	15.46	0.541	
B1	BO-4Cl:L8-BO	0.841	26.15	77.74	17.10	0.530	
Tz6T	eC9-4F	0.860	25.75	67.2	14.9	0.549	33
Tz6T	eC9-4F	0.863	26.12	71.0	16.0	0.520	
BO-1	BTP-eC9	0.845	25.56	77.74	16.79	0.543	34
HD-1	BTP-eC9	0.842	25.61	78.46	17.19	0.556	
OD-1	BTP-eC9	0.828	24.97	71.89	15.18	0.559	
MPhS-C2	BTP-eC9	0.891	26.45	72.82	17.16	0.505	35
MPhS-C2	SSe-NIC	0.876	26.29	73.08	16.83	0.499	
MPhS-C2	BTP-eC9:SSe-NIC	0.880	26.85	76.27	18.02	0.496	
MPhS-C2	L8-S9	0.875	25.69	70.72	15.90	0.543	36
MPhS-C2	L8-BO	0.894	25.37	73.14	16.59	0.538	
MPhS-C2	L8-BO:L8-S9	0.884	26.43	77.46	18.10	0.536	
MPhS-C2	Se-Giant	0.918	25.21	70.34	16.28		This work
MPhS-C2	BTP-eC9	0.892	26.16	73.66	17.19		
MPhS-C2	BTP-eC9:Se-Giant	0.903	26.34	76.33	18.16		

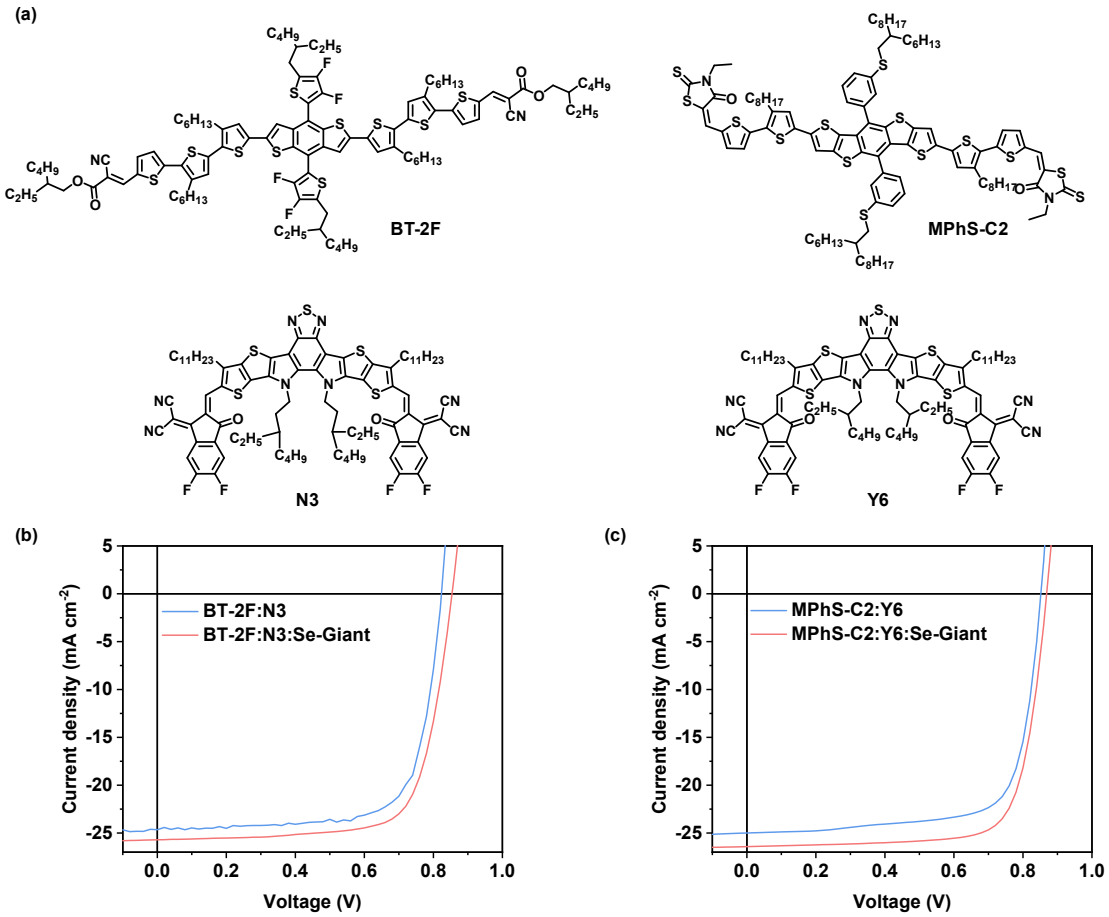

Figure S11. (a) Chemical structures of BT-2F, MPhS-C2, N3 and Y6. (b) The *J-V* curves of the BT-2F:N3, BT-2F:N3:Se-Giant based devices measured under the illumination of AM 1.5G at 100 mW cm^{-2}. (b) The *J-V* curves of the MPhS-C2:Y6, MPhS-C2:Y6:Se-Giant based devices measured under the illumination of AM 1.5G at 100 mW cm^{-2}.

Table S6. Photovoltaic parameters of the BT-2F:N3, BT-2F:N3:Se-giant based devices and the MPhS-C2:Y6, MPhS-C2:Y6:Se-giant based devices measured under the illumination of AM 1.5G at 100 mW cm^{-2}.

Active layer	V_{OC} (V)	J_{SC} (mA cm^{-2})	FF (%)	PCE[a] (%)
BT-2F:N3	0.824	24.66	72.94	14.82 (14.60±0.20)
BT-2F:N3:Se-Giant	0.853	25.70	73.35	16.08 (15.85±0.20)
MPhS-C2:Y6	0.852	25.00	73.96	15.75 (15.70±0.10)
MPhS-C2:Y6:Se-Giant	0.869	26.42	75.96	17.44 (17.15±0.25)

[a)]The average PCE values with standard deviations obtained from ten devices.

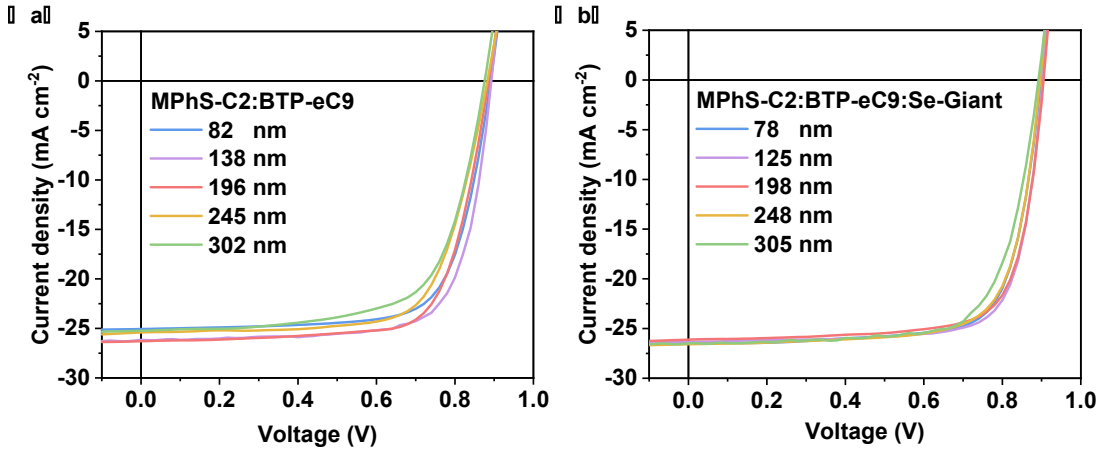

Figure S12. *J-V* characteristics for devices based on (a) MPhS-C2:BTP-eC9 and (b) MPhS-C2:BTP-eC9:Se-Giant, with different active layer thicknesses, measured under the illumination of AM 1.5 G at 100 mW cm^{-2}.

Table S7. Summary of photovoltaic parameters of the all-SMOSCs based on MPhS-C2:BTP-eC9 and MPhS-C2:BTP-eC9:Se-Giant, with different active layer thicknesses, measured under the illumination of AM 1.5 G at 100 mW cm^{-2}.

Systems	Thickness (nm)	V_{OC} (V)	J_{SC} (mA/cm^2)	FF (%)	PCE [a] (%)
MPhS-C2:BTP-eC9	82	0.891	25.06	72.71	16.24 (16.10±0.10)
	138	0.892	26.16	73.66	17.19 (16.98±0.10)
	196	0.886	26.30	72.56	16.91 (16.65±0.20)
	245	0.883	25.41	70.71	15.87 (15.70±0.15)
	302	0.876	25.24	67.56	14.94 (14.80±0.12)
MPhS-C2: BTP-eC9:Se-Giant	78	0.899	26.47	74.61	17.75 (17.60±0.10)
	125	0.903	26.34	76.33	18.16 (18.01±0.12)
	198	0.905	26.15	74.93	17.73 (17.55±0.15)
	248	0.896	26.58	73.59	17.53 (17.25±0.20)
	305	0.892	26.50	71.96	17.01 (16.90±0.05)

[a]The average PCE values with standard deviations were obtained from 10 independent cells.

Table S8. Summary of thickness, PCE and the corresponding photovoltaic parameters of all-SMOSCs

Systems	Thickness (nm)	V_{oc} (V)	J_{sc} (mA/cm^2)	FF (%)	PCE (%)	Reference
DR3TSBDT:$PC_{71}BM$	280	0.88	15.82	65.3	9.05	37
BTR:$PC_{71}BM$	310	0.94	14.5	70	9.5	38
BTR:NITI:$PC_{71}BM$	300	0.94	19.5	73.83	13.63	39
BTR:BTR-OH:$PC_{71}BM$	300	0.93	14.62	74.2	10.14	40
SM1-F:Y6	250	0.85	21.9	64	11.9	17
L2:Y6	300	0.82	24.5	71.2	14.3	41
L1:Y6	300	0.81	24.31	70.5	13.8	
HD1:BTP-eC9	350	0.811	27.25	67.52	14.92	34
T27:Y6	300	0.812	27.21	68.02	15.03	42
DRTB-T-C4:IT-4F	300	0.893	18.68	61.0	10.18	43
BTR:$PC_{71}BM$	250	0.9	13.9	74	9.3	44
DRTT-6Se:N3	300	0.85	25.29	69.9	15.03	45
DRTT-T:N3	300	0.85	22.00	58.6	10.89	
DRTT-2Se:N3	300	0.85	23.33	66.9	13.20	
DRTT-6Se:N3	300	0.84	25.33	64.3	13.81	
C2: $PC_{71}BM$	300	0.97	10.62	56	5.80	46
C4: $PC_{71}BM$	300	0.97	11.43	64	7.17	
NDTP-CNCOO: $PC_{71}BM$	302	0.94	10.77	71.1	7.20	47
	356	0.94	10.49	68.0	6.70	
	413	0.93	10.37	64.7	6.24	
MPhS-C2:BTP-eC9:Se-Giant	305	0.892	26.5	71.96	17.01 (16.90±0.05)	This work

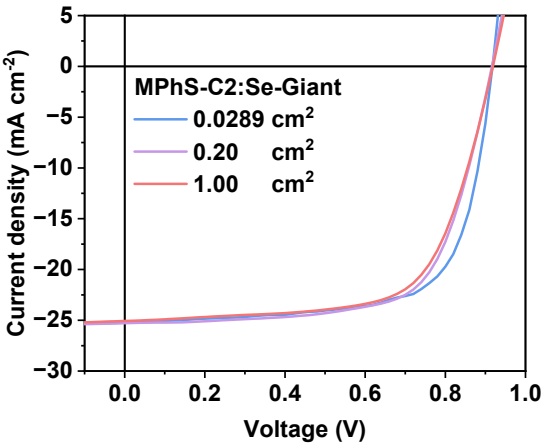

Figure S13. *J-V* characteristics for devices based on MPhS-C2: Se-Giant, with different active layer areas measured under the illumination of AM 1.5 G at 100 mW cm^{-2}.

Table S9. Summary of photovoltaic parameters of the all-SMOSCs based on MPhS-C2:BTP-eC9 with different active layer area, measured under the illumination of AM 1.5 G at 100 mW cm^{-2}.

Area (cm^2)	V_{OC} (V)	J_{SC} (mA/cm^2)	FF (%)	PCE [a] (%)
0.0289	0.918	25.21	70.34	16.28 (16.02±0.12)
0.20	0.916	25.28	68.29	15.82 (15.52±0.20)
1.00	0.918	25.07	66.72	15.35 (14.90±0.22)

[a]The average PCE values with standard deviations were obtained from 10 independent cells.

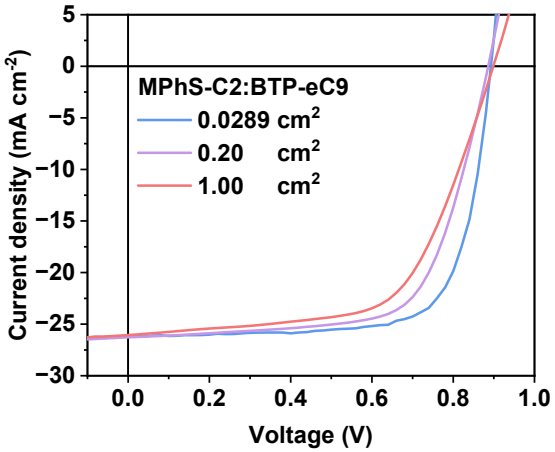

Figure S14. *J-V* characteristics for devices based on MPhS-C2:BTP-eC9, with different active layer areas measured under the illumination of AM 1.5 G at 100 mW cm^{-2}.

Table S10. Summary of photovoltaic parameters of the all-SMOSCs based on MPhS-C2:BTP-eC9 with different active layer area, measured under the illumination of AM 1.5 G at 100 mW cm^{-2}.

Area (cm^2)	V_{OC} (V)	J_{SC} (mA/cm^2)	FF (%)	PCE [a] (%)
0.0289	0.892	26.16	73.66	17.19 (16.98±0.10)
0.20	0.887	26.27	67.53	15.73 (15.45±0.15)
1.00	0.898	26.06	61.53	14.40 (14.22±0.12)

[a]The average PCE values with standard deviations were obtained from 10 independent cells.

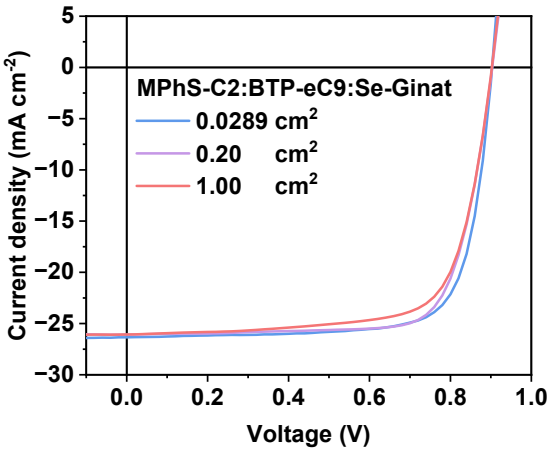

Figure S15. *J-V* characteristics for devices based on MPhS-C2:BTP-eC9:Se-Giant, with different active layer areas measured under the illumination of AM 1.5 G at 100 mW cm^{-2}.

Table S11. Summary of photovoltaic parameters of the all-SMOSCs based on MPhS-C2:BTP-eC9:Se-Giant with different active layer areas, measured under the illumination of AM 1.5 G at 100 mW cm^{-2}.

Area (cm^2)	V_{OC} (V)	J_{SC} (mA/cm^2)	FF (%)	PCE [a] (%)
0.0289	0.903	26.34	76.33	18.16 (18.01±0.12)
0.20	0.903	26.08	75.53	17.78 (17.40±0.12)
1.00	0.902	26.07	72.82	17.12 (17.00±0.08)

[a]The average PCE values with standard deviations were obtained from 10 independent cells.

Table S12. The corresponding T_{80} lifetime of different kinds of OSCs reported in literature.

Active Layer	Systems	PCE (%)	Lifetime (h)	Reference
All-SMOSCs	MPhS-C2:BTP-eC9:Se-Giant	18.16	3000	This work
	MPhS-C2:BTP-eC9	17.19	80	
	MPhS-C2:Se-Giant	16.28	2800	
	MPhS-C2:BTP-eC9:SSe-NIC	18.02	436	[35]
	MPhS-C2:BTP-eC9	17.16	76	
	MPhS-C2:SSe-NIC	16.83	62	
	BTR-Cl:Y6	13.31	8	[48]
	BTR-Cl:Y6	13.88	15	
	B1:Y6	12.32	9	
	B1:Y6	12.76	16	
	B1:BTP-eC9	14.86	14	
	B1:BTP-eC9	13.92	7	
	BTR-F:M36	10.14	0.38	[49]
	BTR-F:M36:N2200	12.19	0.66	
	DRCN5T:$PC_{71}BM$	6.73	1375.6	[50]
	DRCN5T:$PC_{71}BM$	8.87	870	
	DRCN5T:$PC_{71}BM$	6.64	192	
	BTR:$PC_{71}BM$	9.81	78	[51]
	BTR:$PC_{71}BM$	10.14	50	
	BTR:$PC_{71}BM$	9.16	15	
	BTR:$PC_{71}BM$	7.12	8	
	BTR:$PC_{71}BM$	6.59	65	
	SM-BDT:Y8	10.68	96	[52]
	SM-DTBDT:Y8	12.45	756	
	X2:$PC_{61}BM$	6.3	88	[53]
	F3:$PC_{61}BM$	7.3	82	
	DRCN7T:$PC_{71}BM$	9.1	86	
	MPhS-C2:L8-BO	16.59	124	[36]
	MPhS-C2: L8-S9	15.9	595	
	MPhS-C2:L8-BO :L8-S9	18.1	993	

Operational stability measurements: The devices were fabricated without further encapsulation. We measured light-induced degradation experiments with one sun equivalent illumination intensity for 800 hours. The devices were put inside a nitrogen filled glovebox (H_2O < 1 ppm, O_2 < 1 ppm) and continuously illuminated with a white LED array (XLamp CXA1512 6500K CCT). The illumination light intensity was initially set before testing to make sure the output short-circuit current density equals the value that was measured under standard conditions mentioned earlier, and it monitored by a photodiode (Hamamtsu S1336-8BQ) to guarantee stable light intensity. *J-V* characters of the devices were checked periodically, and the photovoltaic parameters were calculated automatically according to the achieved *J-V* curves. Notably, the photovoltaic parameters of devices under illumination were recorded overtime and the degradation curves were shown.

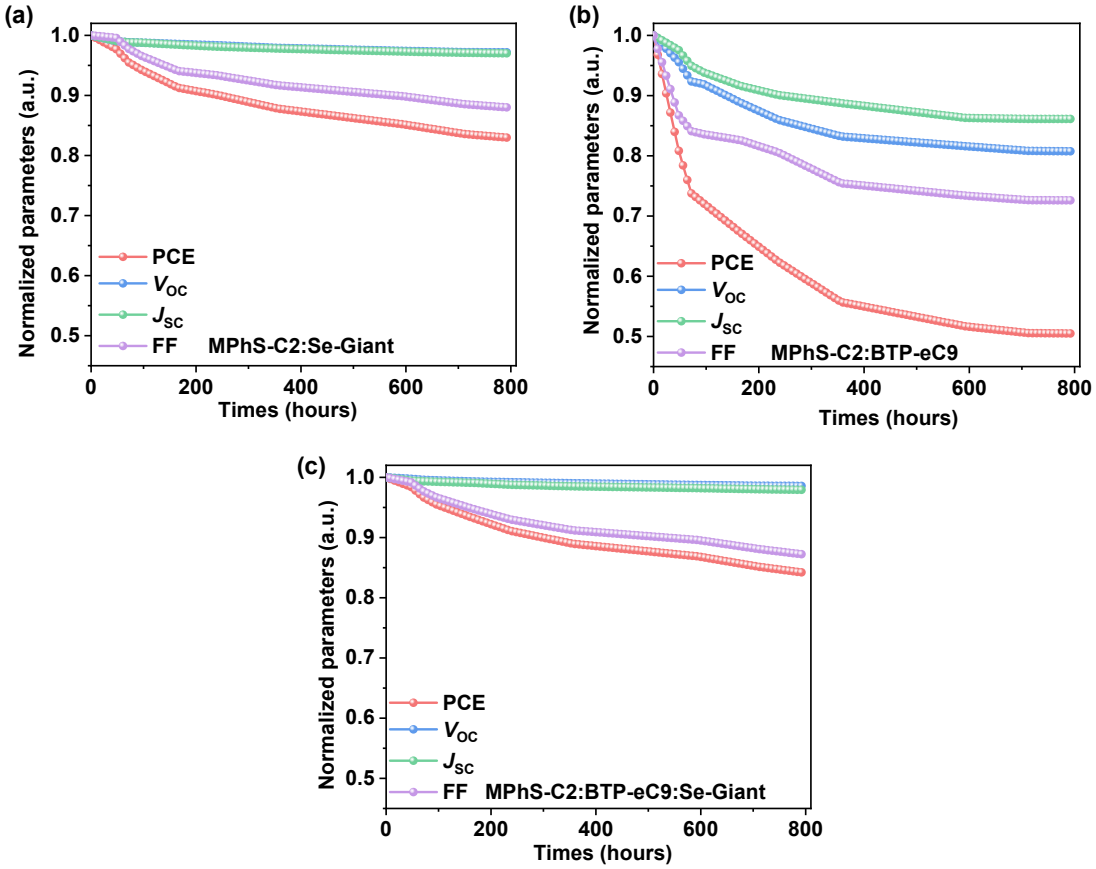

Figure S16. The normalized degradation trends of relevant photovoltaic parameters including PCE, FF, J_{SC} and V_{OC} under continuous light-soaking for (a) MPhS-C2:Se-Giant, (b) MPhS-C2:BTP-eC9 and (c) MPhS-C2:BTP-eC9:Se-Giant.

Thermal stability testing: The testing devices were fabricated under the same preparation conditions, as mentioned above. After the spin-coating of the active layer deposited on the ITO/PEDOT:PSS films, the samples were transferred to a hot plate at 100 °C in a N_2-filled glovebox and annealed for various time periods. Then, the samples were quenched to room temperature before the cathode layers were thermally deposited. All the samples for time-dependent annealing measurements were prepared under the same conditions with the thermal stability testing ones.

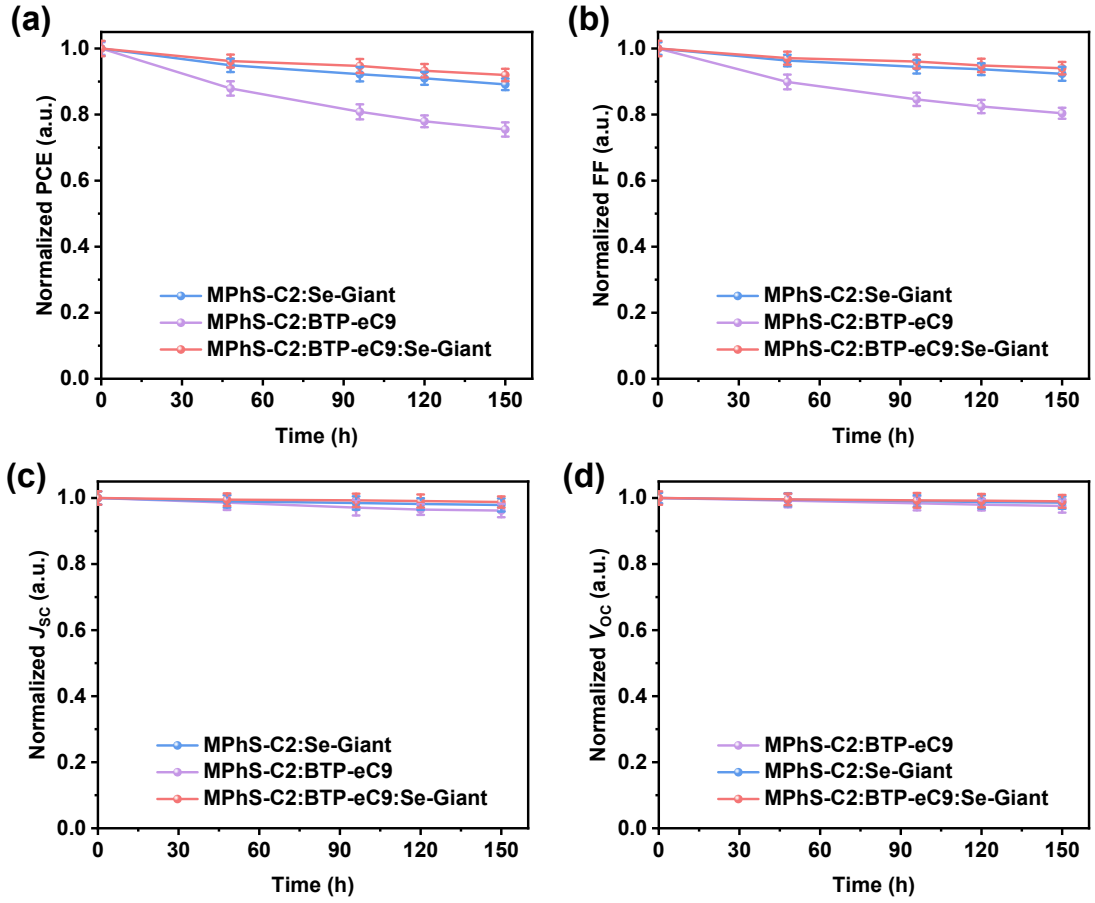

Figure S17. The normalized degradation trends of relevant photovoltaic parameters of the MPhS-C2:Se-Giant, MPhS-C2:BTP-eC9, MPhS-C2:BTP-eC9:Se-Giant including (a) PCE, (b) FF, (c) J_{SC}, (d) V_{OC}, under continuous thermal annealing.

Diffusion ordered spectroscopy (DOSY): The Bruker AVANCE (600 MHz) was applied to obtain diffusion ordered spectroscopy (DOSY) in solution. The experiment was conducted at room temperature, for which the concentration is 12 mg/mL for BTP-eC9 and 15 mg/mL for BTP-eC9:Se-Giant (0.8:0.2, wt%). The diffusion coefficient was calculated by Stokes-Einstein equation:

$$D = \frac{kT}{6\pi\eta r_s}$$

Where D is diffusion coefficient, k is Boltzmann constant, T is temperature, η is viscosity of solvent and r_s is the thermodynamic radius of the molecule. Generally, larger D indicates stronger molecular diffusion.

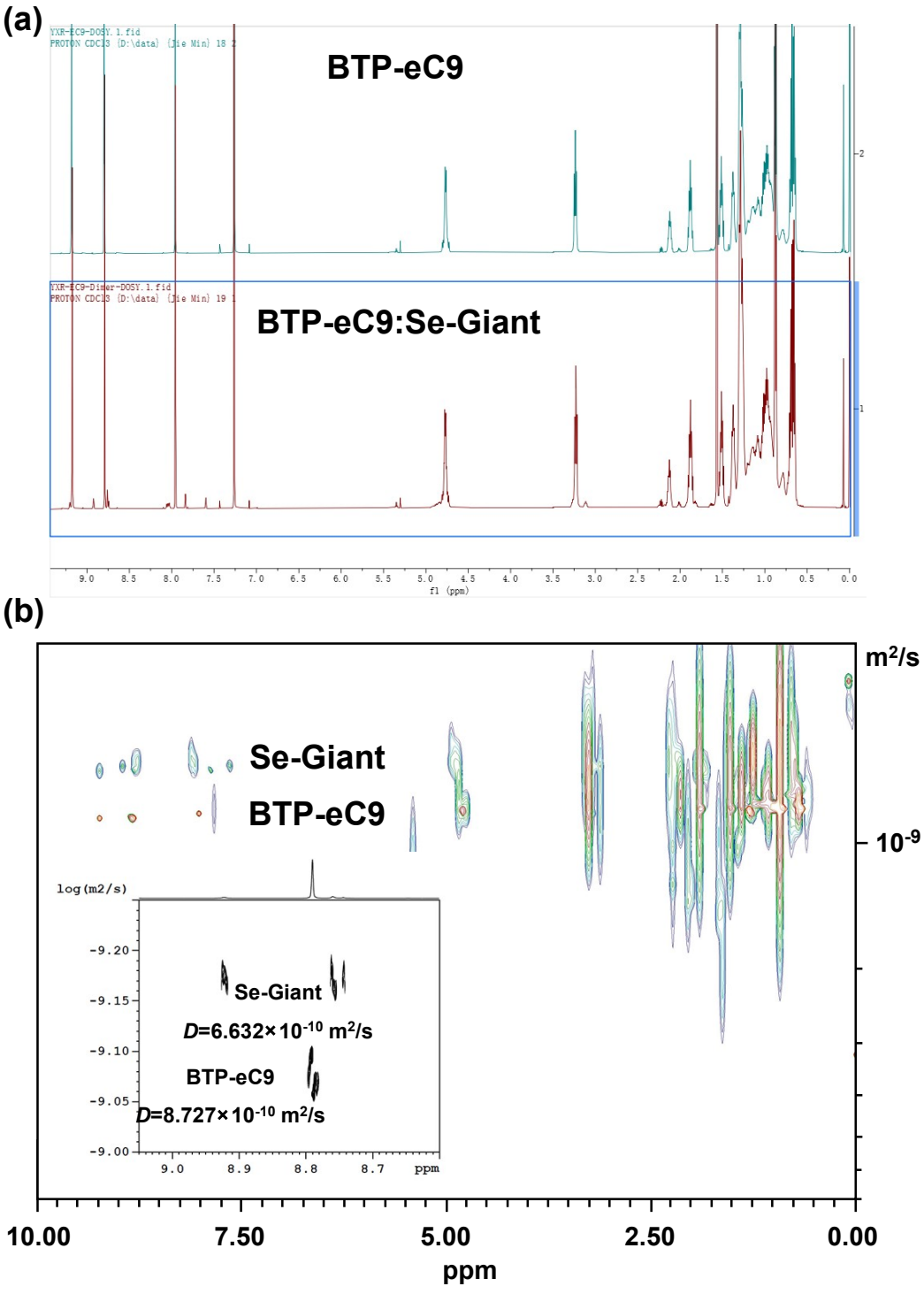

Figure S18. (a) ^{1}H NMR spectra of BTP-eC9 and BTP-eC9:Se-Giant in $CDCl_3$ solution. (b) ^{1}H DOSY spectra of BTP-eC9:Se-Giant in $CDCl_3$ solution.

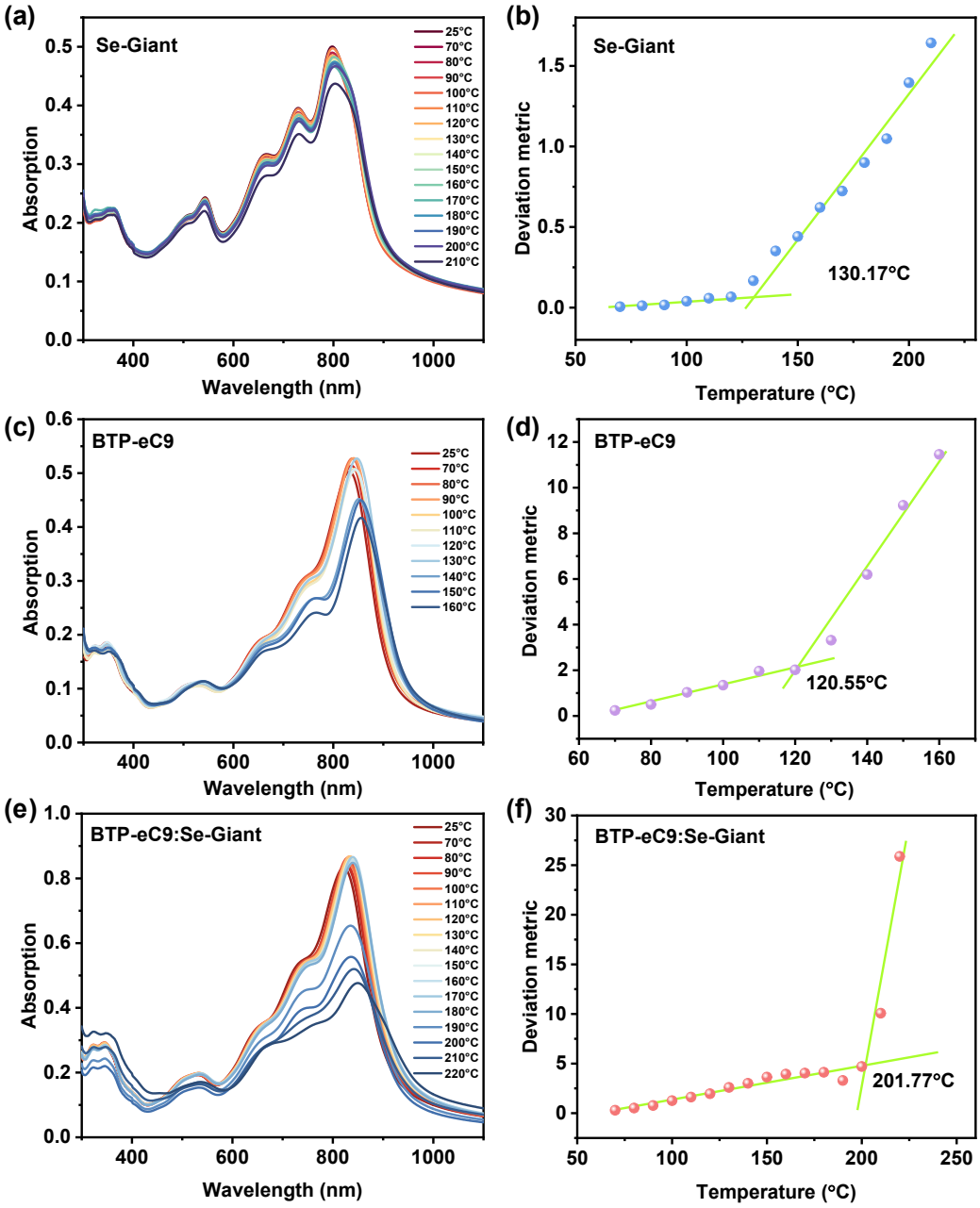

Figure S19. *UV–vis-NIR* absorption spectra of (a) Se-Giant, (c) BTP-eC9 and (e) BTP-eC9:Se-Giant. Evolution of the deviation Metric (DM_T) as a function of annealing temperature, illustrating a glass transition of (b) Se-Giant (130.17 °C), (d) BTP-eC9 (120.55 °C) and (f) BTP-eC9:Se-Giant (201.77 °C). Notably, the DM_T factor represents the sum of squared deviations in absorbance between un-annealed and annealed films:[54, 55] $DM_T = \sum_{\lambda_{min}}^{\lambda_{max}} [(I_{RT}(\lambda) - I_T(\lambda)]^2$, where λ, λ_{min} and λ_{max} are explained as the wavelength, the lower and upper bounds of the optical sweep, $I_{RT}(\lambda)$ and $I_T(\lambda)$ are explained as the normalized absorption intensities of un-annealed and annealed films, respectively. When the overall absorption intensity changes significantly, it suggests

that the inherent properties of the material have undergone a glass transition, and the corresponding temperature is T_g.

***Transient absorption spectroscopy (TAS)*:** For femtosecond transient absorption spectroscopy, the fundamental output from Yb:KGW laser (1030 nm, 220 fs Gaussian fit, 100 kHz, Light Conversion Ltd) was separated into two light beams. One was introduced to NOPA (ORPHEUS-N, Light Conversion Ltd) to produce a certain wavelength for the pump beam (here we use 825 nm), and the other was focused onto a YAG plate to generate a white light continuum as a probe beam. The pump and probe overlapped on the sample at a small angle of less than 10°. The transmitted probe light from the sample was collected by a linear CCD array. Then we obtained transient differential, transmission signals by the equation shown below:

$$\frac{\Delta T}{T} = \frac{T_{pump-on} - T_{pump-off}}{T_{pump-off}}$$

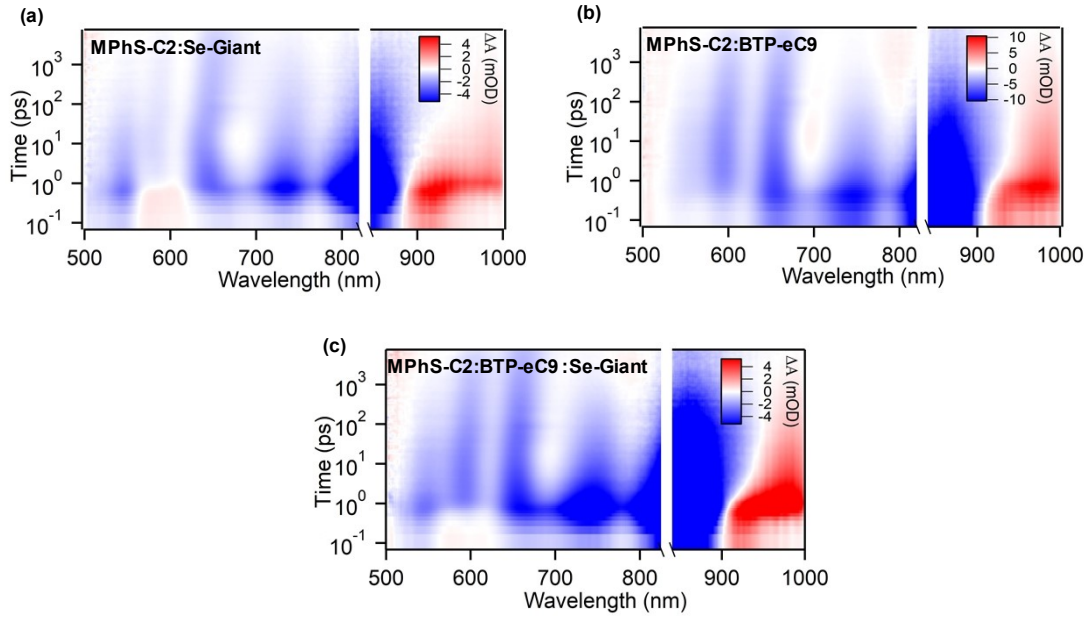

Figure S20. The TA images of a) MPhS-C2:Se-Giant film, b) MPhS-C2:BTP-eC9 film, and c) MPhS-C2:BTP-eC9:Se-Giant film under 825 nm pump.

Table S13. Parameters constants of A1, τ_1, and A2 τ_2 of different blends.

Systems	A1	τ_1 (ps)	A2	τ_2 (ps)	Average τ_h (ps)
MPhS-C2:Se-Giant	55.2	0.58	44.8	10.88	5.19
MPhS-C2:BTP-eC9	53.1	0.46	46.9	10.40	5.12

MPhS-C2: BTP-eC9:Se-Giant	54.8	0.45	45.2	9.75	4.66

***Transient photocurrent (TPC) measurements*:** Relevant control and MSM solar cells were excited with a 405 nm laser diode. The transient photocurrent response of the devices at a short circuit condition to a 200 μs square pulse from the LED with no background illumination. The current traces were recorded on a Tektronix DPO3034 digital oscilloscope by measuring the voltage drop over a 5-ohm sensor resistor in series with the solar cell. DC voltage was applied to the solar cell with an MRF544 bipolar junction transistor in a common collector amplifier configuration.

***Transient photovoltage (TPV) measurements*:** In the TPV measurements, a 405 nm laser diode was used to keep the organic solar cells in the V_{OC} conditions. Measuring the light intensity with a highly linear photodiode and driving the laser intensity with a waveform generator (Agilent 33500B). Moreover, a small perturbation was induced with a second 405 nm laser diode. The intensity of the short laser pulse was adjusted to keep the voltage perturbation below 10 mV. After the pulse, the voltage decays back to its steady state value in a single exponential decay.

Table S14. The exciton generation, charge collection, charge recombination and charge extraction lifetime of the binary and ternary devices.

Systems	η_{diss}[a] (%)	η_{coll}[b] (%)	α[c]	n (kT/q)[d]	τ_{TPC}[e]	τ_{TPV}[f]
MPhS-C2:Se-Giant	96.20	80.50	0.993	1.25	3.2	1.89
MPhS-C2: BTP-eC9	96.52	83.22	0.991	1.41	2.7	4.23
MPhS-C2: BTP-eC9:Se-Giant	98.08	87.58	0.996	1.18	1.1	6.76

[a]Under short circuit condition. [b]Under the maximal power output condition. [c]$J_{sc} \propto P_{in}^{\alpha}$. [d]$V_{oc} \propto (nkT/q)\ln P_{in}$. [e]The extraction time extract from TPC. [f]The extracted carrier lifetimes extract from TPV.

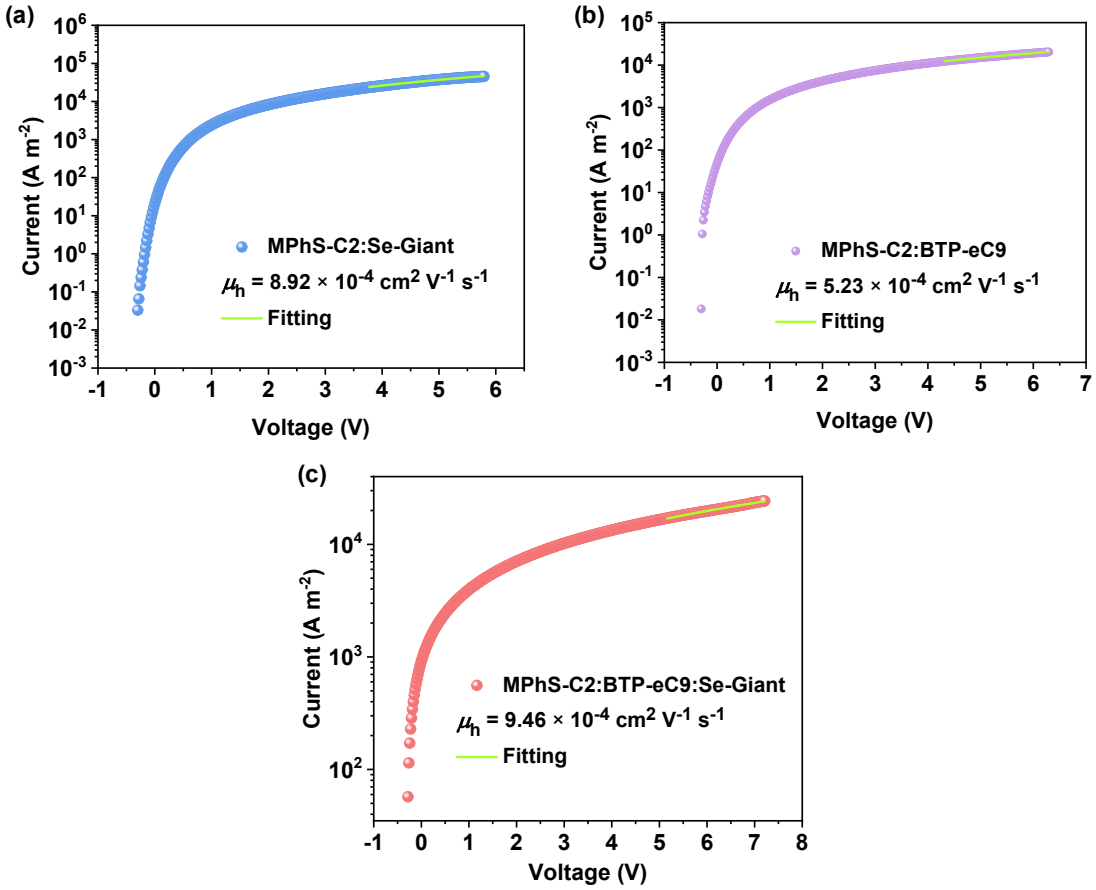

Figure S21. The dark *J-V* characteristics of the (a) MPhS-C2:Se-Giant, (b) MPhS-C2:BTP-eC9 and (c) MPhS-C2: BTP-eC9:Se-Giant based hole-only devices. The green lines represent the best fitting using the SCLC model.

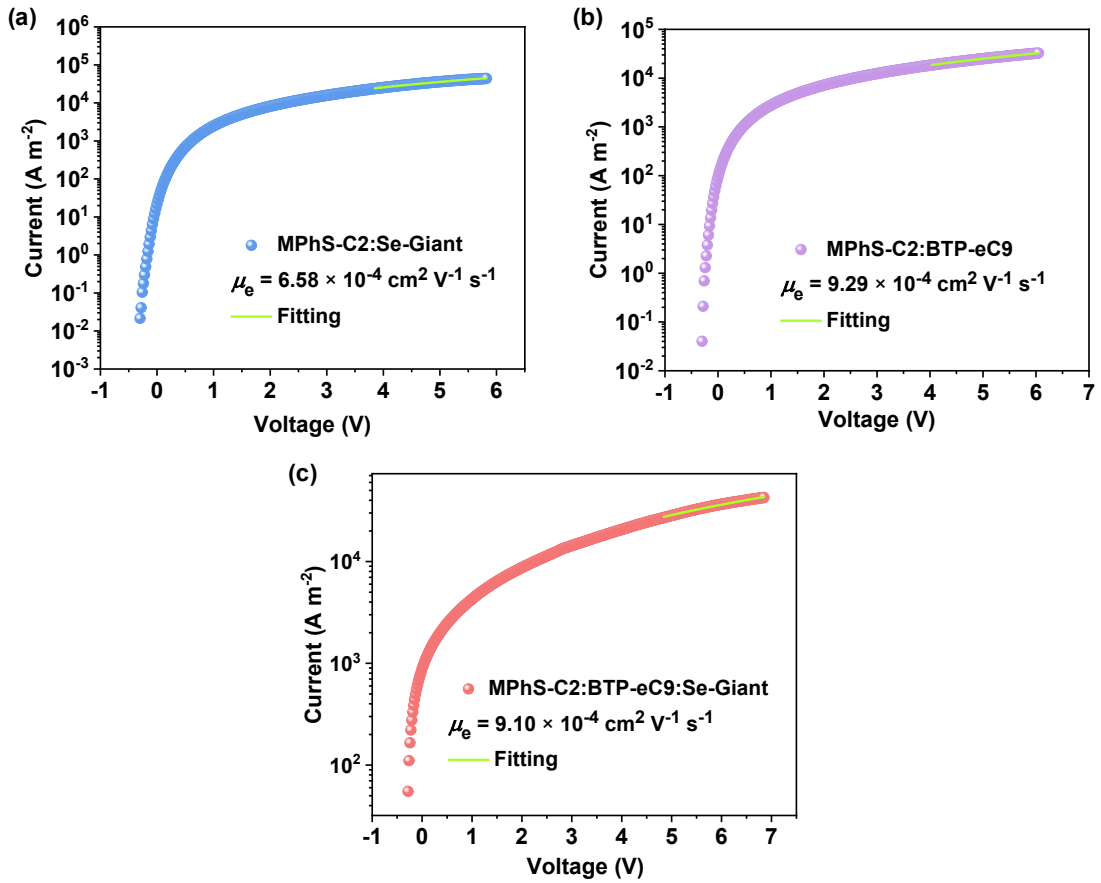

Figure S22. The dark *J-V* characteristics of the (a) MPhS-C2:Se-Giant, (b) MPhS-C2:BTP-eC9 and (c) MPhS-C2: BTP-eC9:Se-Giant based electron-only devices. The green lines represent the best fitting using the SCLC model.

Table S15. Investigations of the hole and electron mobilities and corresponding μ_h/μ_e ratios of the relevant devices extracted from the SCLC measurements and device mobilities.

Systems	Hole mobility ($\times 10^{-4}$ cm^2 V^{-1} s^{-1})	Electron mobility ($\times 10^{-4}$ cm^2 V^{-1} s^{-1})	μ_h/μ_e
MPhS-C2:Se-Giant	8.92	6.58	1.35
MPhS-C2:BTP-eC9	5.23	9.29	0.66
MPhS-C2: BTP-eC9:Se-Giant	9.46	9.10	0.86

***FTPS-EQE spectra measurements*:** FTPS-EQE measurement was performed at a Vertex 70 from Bruker Optics, which is equipped with a quartz tungsten halogen lamp, quartz beam-splitter, and external detector option. The amplification of the photocurrent product was achieved by using a low-noise current amplifier (SR570) on the illumination of the photovoltaic devices with light modulated by the Fourier transform infrared spectroscopy (FTIR). The external detector port of the FTIR gathered the signals from the current amplifier for output voltage. A Keithley 2400 Source Meter was used for supplying voltages and recording injected current, and a Keithley 485 picoammeter was used for measuring the emitted light intensity.

***Electroluminescence (EL) measurement*:** The EL signature was collected with a monochromator and detected with an InGaAs detector. The data collection range is 700-1300 nm.

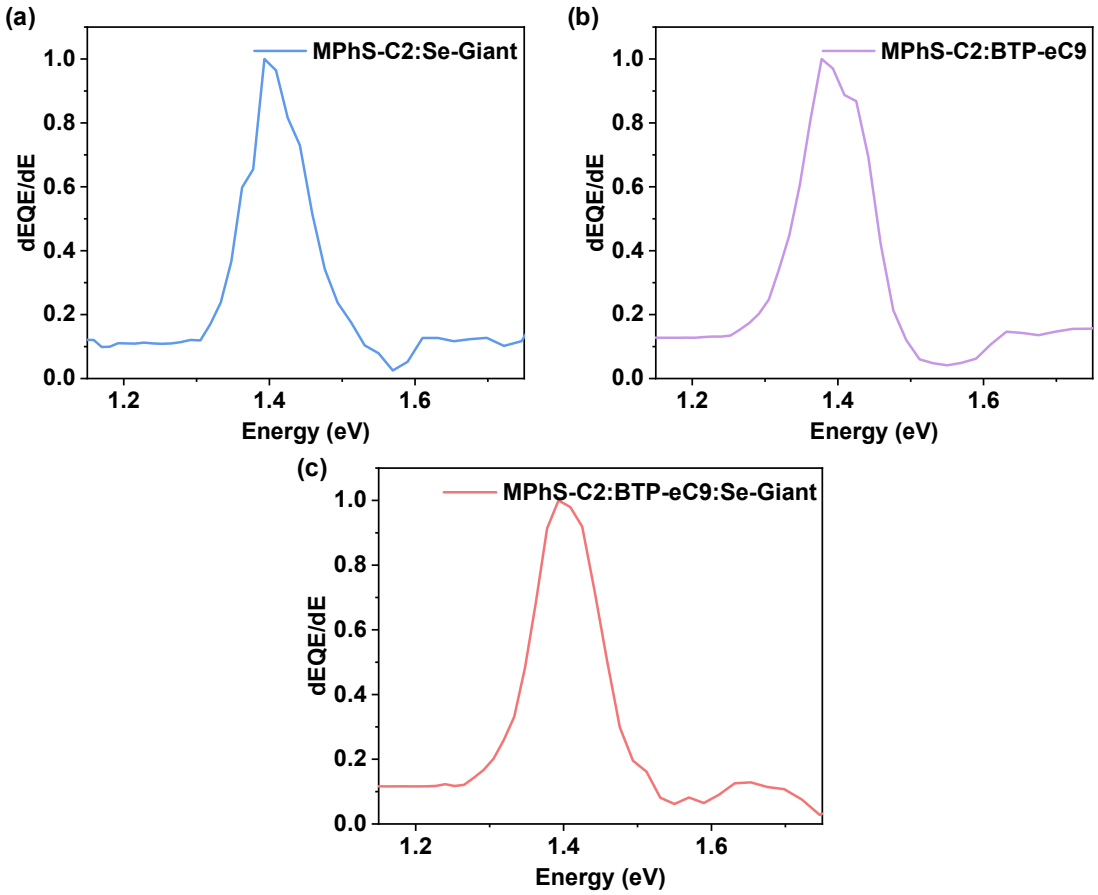

Figure S23. Bandgap distributions for all-SMOSCs based on (a) MPhS-C2:Se-Giant, (b) MPhS-C2:BTP-eC9, and (c) MPhS-C2:BTP-eC9:Se-Giant blends. The E_g value is determined by the derivatives of the FTPS-EQE curve and then calculated according to the literature[36].

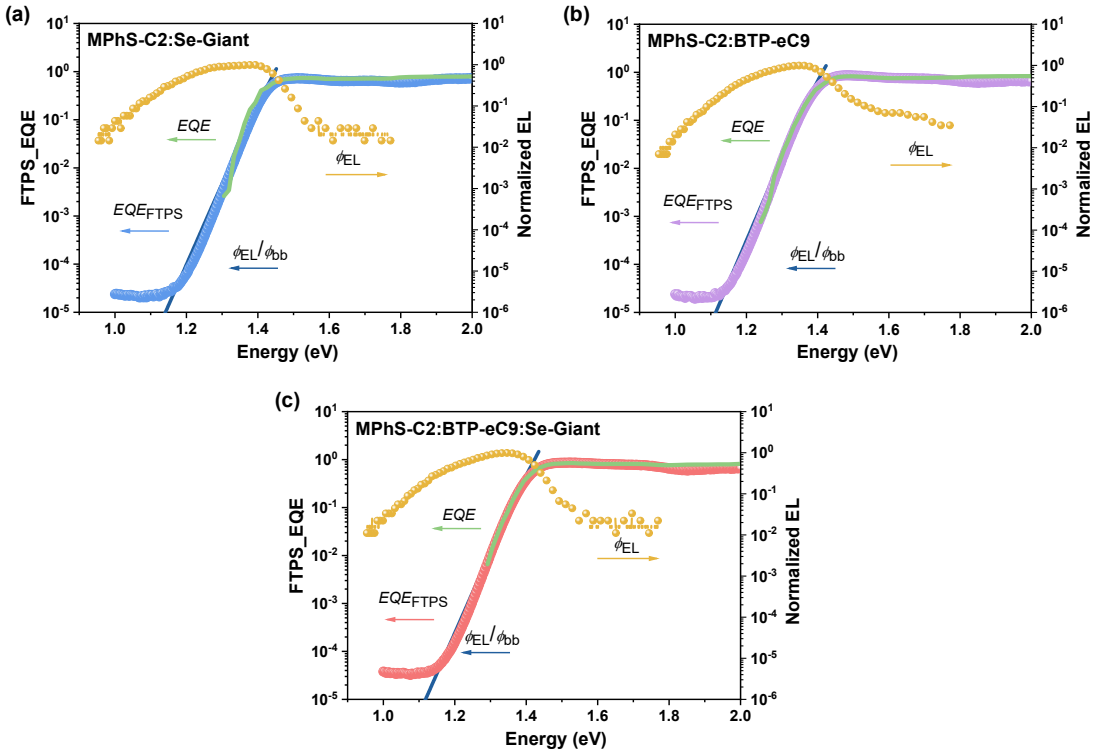

Figure S24. Semilogarithmic plots of normalized EL spectra, measured EQE spectra, and FTPS-EQE spectra as a function of energy for devices based on (a) MPhS-C2:Se-Giant, (b) MPhS-C2:BTP-eC9, and (c) MPhS-C2:BTP-eC9:Se-Giant blends.

EQE-EL Measurement: *Electroluminescence (EL) quantum efficiency (EQEEL) measurements were performed by applying external voltage sources through the devices from 1V to 3V. A Keithley 2400 Source Meter was used for supplying voltages and recording injected current, and a Keithley 485 picoammeter was used for measuring the emitted light intensity.*

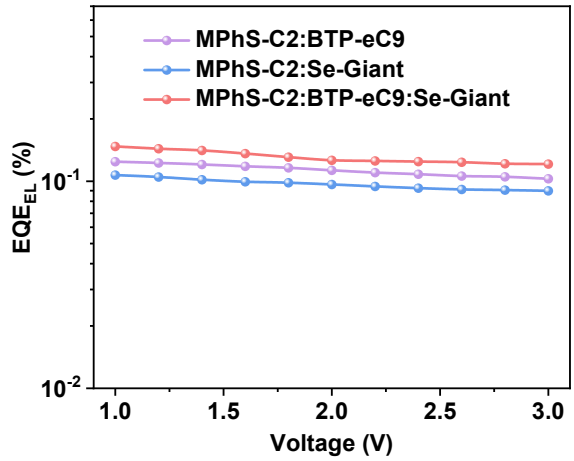

Figure S25. The EQE_{EL} of the binary and ternary devices at different injected voltages.

Table S16. Measured and calculated parameters to quantify the non-radiative recombination losses of the binary and ternary devices.

Systems	E_g[a] (eV)	V_{oc}[b] (V)	E_{loss} (eV)	VSQ oc (V)	ΔE_1 (eV)	Vrad oc[c] (V)	ΔE_2 (eV)	ΔE_3 (eV)	EQE_{EL}[d] (%)	$Exp.\Delta E_3$[e] (eV)
MPhS-C2:Se-Giant	1.408	0.918	0.490	1.147	0.261	1.091	0.056	0.173	0.097	0.179
MPhS-C2:BTP-eC9	1.396	0.893	0.503	1.142	0.254	1.061	0.081	0.168	0.113	0.175
MPhS-C2:BTP-eC9:Se-Giant	1.402	0.903	0.499	1.146	0.256	1.067	0.078	0.165	0.131	0.170

[a]E_{gap} was determined from the curve of the dEQE/dE. [b]V_{oc} was calculated from the measured *J-V* curves. [c]V_{oc}^{rad} was calculated from FTPS and EL measurements. [d]EQE_{EL} is the EL quantum efficiency of the fabricated devices; [e]Exp.ΔE_3 is calculated with the Equation ($\Delta E_3 = -kTln(EQE_{EL})$).

***Atomic force microscopy (AFM) measurements*:** AFM measurements were performed by using a Nano Wizard 4 atomic force microscopy (JPK Inc. Germany) in Qi mode to observe the surface morphologies of the ITO/PEDOT:PSS/active layer.

Table S17. Investigations of the morphology parameters extracted from the GIWAXS measurements of MPhS-C2:Se-Giant, MPhS-C2:BTP-eC9 and MPhS-C2:BTP-eC9:Se-Giant blends.

Systems	In plane				Out of plane			
	Lamellar stacking (100)				π-π stacking (010)			
	q (Å^{-1})	*d* (Å)	FWHM (Å^{-1})	CCL (Å)	*q* (Å^{-1})	*d* (Å)	FWHM (Å^{-1})	CCL (Å)
MPhS-C2:Se-Giant	0.27	23.71	0.062	101.34	1.79	3.50	0.33	18.92
MPhS-C2:BTP-eC9	0.26	24.17	0.060	104.72	1.83	3.44	0.32	19.33
MPhS-C2:BTP-eC9:Se-Giant	0.27	23.71	0.061	103.00	1.83	3.43	0.36	17.55

***Grazing incidence small angle X-ray scattering (GISAXS) characterization*:** GISAXS measurements with Kα X-ray of Cu source (8.05 keV, 1.54 Å) and a Pilatus3R 300 K detector were conducted at a Xeuss 2.0 SAXS laboratory beamline. Samples were prepared by spin coating identical chloroform blend solutions as those used in devices on Si substrates. The grazing incident angle was 0.18°.

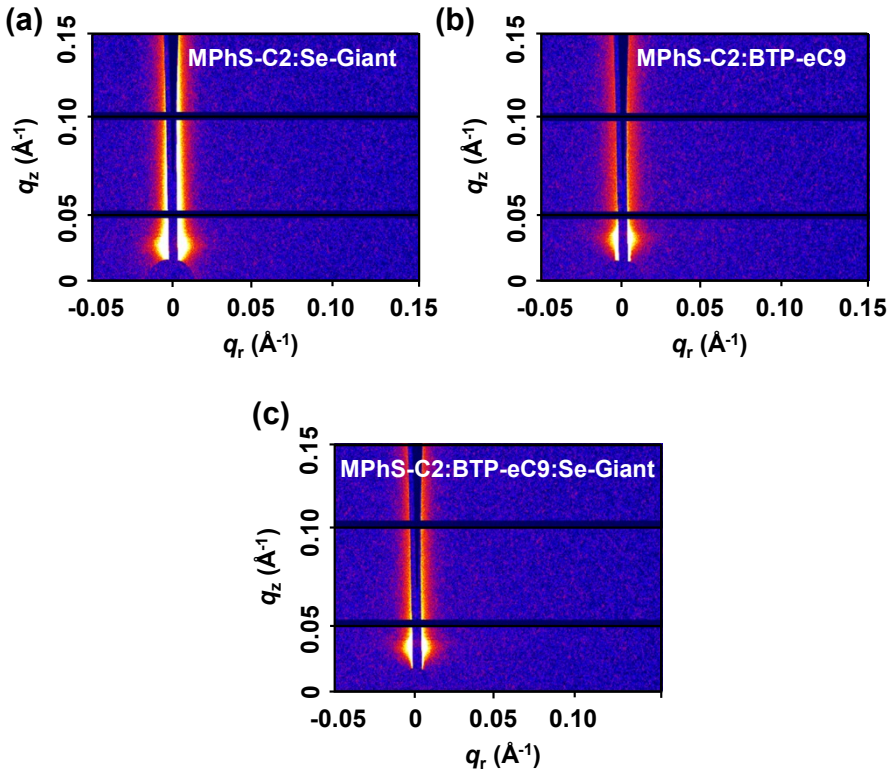

Figure S26. Relevant results of GISAXS measurement on (a) MPhS-C2:Se-Giant, (b) MPhS-C2:BTP-eC9, and (C) MPhS-C2:BTP-eC9:Se-Giant blend films.

References

1. J. Yuan, Y. Zhang, L. Zhou, G. Zhang, H.-L. Yip, T.-K. Lau, X. Lu, C. Zhu, H. Peng, P. A. Johnson, M. Leclerc, Y. Cao, J. Ulanski, Y. Li and Y. Zou, *Joule*, 2019, **3**, 1140-1151.
2. X. Yang, R. Sun, Y. Wang, M. Chen, X. Xia, X. Lu, G. Lu and J. Min, *Adv. Mater.*, 2022, **35**, 2209350.
3. D. K. Owens and R. C. Wendt, *J. Appl. Polym. Sci.*, 2003, **13**, 1741-1747.
4. A. B. Svante Nilsson, Andrzej Budkowski, and Ellen Moons, *Macromolecules*, 2007, **40**, 8291-8301.
5. L. Zhang, D. Deng, K. Lu and Z. Wei, *Adv. Mater.*, 2024, **36**, 2302915.
6. H. Bin, Y. Yang, Z.-G. Zhang, L. Ye, M. Ghasemi, S. Chen, Y. Zhang, C. Zhang, C. Sun, L. Xue, C. Yang, H. Ade and Y. Li, *J. Am. Chem. Soc.*, 2017, **139**, 5085-5094.
7. M. A. Adil, J. Zhang, D. Deng, Z. Wang, Y. Yang, Q. Wu and Z. Wei, *ACS Appl. Mater. Interfaces*, 2018, **10**, 31526-31534.
8. H. Li, Y. Zhao, J. Fang, X. Zhu, B. Xia, K. Lu, Z. Wang, J. Zhang, X. Guo and Z. Wei, *Adv. Energy Mater.*, 2018, **8**, 1702377.
9. L. Xiao, T. Lai, X. Liu, F. Liu, T. P. Russell, Y. Liu, F. Huang, X. Peng and Y. Cao, *J. Mater. Chem. A*, 2018, **6**, 18469-18478.
10. K. Gao, S. B. Jo, X. Shi, L. Nian, M. Zhang, Y. Kan, F. Lin, B. Kan, B. Xu, Q. Rong, L. Shui, F. Liu, X. Peng, G. Zhou, Y. Cao and A. K. Y. Jen, *Adv. Mater.*, 2019, **31**, 1807842.
11. Q. Yue, H. Wu, Z. Zhou, M. Zhang, F. Liu and X. Zhu, *Adv. Mater.*, 2019, **31**, 1904283.
12. H. Chen, D. Hu, Q. Yang, J. Gao, J. Fu, K. Yang, H. He, S. Chen, Z. Kan, T. Duan, C. Yang, J. Ouyang, Z. Xiao, K. Sun and S. Lu, *Joule*, 2019, **3**, 3034-3047.
13. R. Zhou, Z. Jiang, C. Yang, J. Yu, J. Feng, M. A. Adil, D. Deng, W. Zou, J.

Zhang, K. Lu, W. Ma, F. Gao and Z. Wei, *Nat. Commun.*, 2019, **10**, 5393.

14. Q. Wu, D. Deng, J. Zhang, W. Zou, Y. Yang, Z. Wang, H. Li, R. Zhou, K. Lu and Z. Wei, *Sci. China Chem.*, 2019, **62**, 837-844.
15. Q. Wu, D. Deng, R. Zhou, J. Zhang, W. Zou, L. Liu, S. Wu, K. Lu and Z. Wei, *ACS Appl. Mater. Interfaces*, 2020, **12**, 25100-25107.
16. R. Zhou, Z. Jiang, Y. Shi, Q. Wu, C. Yang, J. Zhang, K. Lu and Z. Wei, *Adv. Funct. Mater.*, 2020, **30**, 2005426.
17. B. Qiu, Z. Chen, S. Qin, J. Yao, W. Huang, L. Meng, H. Zhu, Y. Yang, Z. G. Zhang and Y. Li, *Adv. Mater.*, 2020, **32**, 1908373.
18. J. Ge, L. Xie, R. Peng, B. Fanady, J. Huang, W. Song, T. Yan, W. Zhang and Z. Ge, *Angew. Chem. Int. Ed.*, 2020, **59**, 2808-2815.
19. J. Qin, C. An, J. Zhang, K. Ma, Y. Yang, T. Zhang, S. Li, K. Xian, Y. Cui, Y. Tang, W. Ma, H. Yao, S. Zhang, B. Xu, C. He and J. Hou, *Sci. China Mater.*, 2020, **63**, 1142-1150.
20. J. Ge, L. Hong, W. Song, L. Xie, J. Zhang, Z. Chen, K. Yu, R. Peng, X. Zhang and Z. Ge, *Adv. Energy Mater.*, 2021, **11**, 2100800.
21. J. Qin, Z. Chen, P. Bi, Y. Yang, J. Zhang, Z. Huang, Z. Wei, C. An, H. Yao, X. Hao, T. Zhang, Y. Cui, L. Hong, C. Liu, Y. Zu, C. He and J. Hou, *Energy Environ. Sci.*, 2021, **14**, 5903-5910.
22. X. Wang, J. Wang, J. Han, D. Huang, P. Wang, L. Zhou, C. Yang, X. Bao and R. Yang, *Nano Energy*, 2021, **81**, 105612.
23. S. Cai, P. Huang, G. Cai, X. Lu, D. Hu, C. Hu and S. Lu, *ACS Appl. Mater. Interfaces*, 2022, **14**, 14532-14540.
24. L. Zhang, X. Zhu, D. Deng, Z. Wang, Z. Zhang, Y. Li, J. Zhang, K. Lv, L. Liu, X. Zhang, H. Zhou, H. Ade and Z. Wei, *Adv. Mater.*, 2021, **34**, 2106316.
25. J. Ge, L. Hong, H. Ma, Q. Ye, Y. Chen, L. Xie, W. Song, D. Li, Z. Chen, K. Yu, J. Zhang, Z. Wei, F. Huang and Z. Ge, *Adv. Mater.*, 2022, **34**, 2202752.
26. L. Zhang, R. Sun, Z. Zhang, J. Zhang, Q. Zhu, W. Ma, J. Min, Z. Wei and D. Deng, *Adv. Mater.*, 2022, **34**, 2207020.

27. W. Gao, M. Jiang, Z. Wu, B. Fan, W. Jiang, N. Cai, H. Xie, F. R. Lin, J. Luo, Q. An, H. Y. Woo and A. K. Y. Jen, *Angew. Chem. Int. Ed.*, 2022, **61**, e202205168.

28. Y. Chang, X. Zhu, Y. Shi, Y. Liu, K. Meng, Y. Li, J. Xue, L. Zhu, J. Zhang, H. Zhou, W. Ma, Z. Wei and K. Lu, *Energy Environ. Sci.*, 2022, **15**, 2937-2947.

29. Z. Li, X. Wang, N. Zheng, A. Saparbaev, J. Zhang, C. Xiao, S. Lei, X. Zheng, M. Zhang, Y. Li, B. Xiao and R. Yang, *Energy Environ. Sci.*, 2022, **15**, 4338-4348.

30. S. Wu, W. Feng, L. Meng, Z. Zhang, X. Si, Y. Chen, X. Wan, C. Li, Z. Yao and Y. Chen, *Nano Energy*, 2022, **103**, 107801.

31. L. Meng, M. Li, G. Lu, Z. Shen, S. Wu, H. Liang, Z. Li, G. Lu, Z. Yao, C. Li, X. Wan and Y. Chen, *Small*, 2022, **18**, 2201400.

32. M. Jiang, H.-F. Zhi, B. Zhang, C. Yang, A. Mahmood, M. Zhang, H. Y. Woo, F. Zhang, J.-L. Wang and Q. An, *ACS Energy Lett.*, 2023, **8**, 1058-1067.

33. D. Hu, H. Tang, S. Karuthedath, Q. Chen, S. Chen, J. I. Khan, H. Liu, Q. Yang, J. Gorenflot, C. E. Petoukhoff, T. Duan, X. Lu, F. Laquai and S. Lu, *Adv. Funct. Mater.*, 2022, **33**, 2211873.

34. K. Ma, W. Feng, H. Liang, H. Chen, Y. Wang, X. Wan, Z. Yao, C. Li, B. Kan and Y. Chen, *Adv. Funct. Mater.*, 2023, **33**, 2214926.

35. Y. Gao, X. Yang, W. Wang, R. Sun, J. Cui, Y. Fu, K. Li, M. Zhang, C. Liu, H. Zhu, X. Lu and J. Min, *Adv. Mater.*, 2023, **35**, 2300531.

36. Y. Gao, X. Yang, R. Sun, L.-Y. Xu, Z. Chen, M. Zhang, H. Zhu and J. Min, *Joule*, 2023, **7**, 2845-2858.

37. Q. Zhang, B. Kan, X. Wan, H. Zhang, F. Liu, M. Li, X. Yang, Y. Wang, W. Ni, T. P. Russell, Y. Shen and Y. Chen, *J. Mater. Chem. A*, 2015, **3**, 22274-22279.

38. A. Armin, J. Subbiah, M. Stolterfoht, S. Shoaee, Z. Xiao, S. Lu, D. J. Jones and P. Meredith, *Adv. Energy Mater.*, 2016, **6**, 1600939.

39. Z. Zhou, S. Xu, J. Song, Y. Jin, Q. Yue, Y. Qian, F. Liu, F. Zhang and X. Zhu, *Nat. Energy*, 2018, **3**, 952-959.

40. H. Tang, T. Xu, C. Yan, J. Gao, H. Yin, J. Lv, R. Singh, M. Kumar, T. Duan, Z.

Kan, S. Lu and G. Li, *Adv. Sci.*, 2019, **6**, 1901613.

41. T. Xu, J. Lv, K. Yang, Y. He, Q. Yang, H. Chen, Q. Chen, Z. Liao, Z. Kan, T. Duan, K. Sun, J. Ouyang and S. Lu, *Energy Environ. Sci.*, 2021, **14**, 5366-5376.
42. T. Xu, J. Lv, D. Zheng, Z. Luo, M. H. Jee, G. Ran, Z. Chen, Z. Huang, J. Ren, Y. Li, C. e. Zhang, H. Hu, T. Pauporté, W. Zhang, H. Y. Woo and C. Yang, *Energy Environ. Sci.*, 2023, **16**, 5933-5943.
43. L. Yang, S. Zhang, C. He, J. Zhang, Y. Yang, J. Zhu, Y. Cui, W. Zhao, H. Zhang, Y. Zhang, Z. Wei and J. Hou, *Chem. Mater.*, 2018, **30**, 2129-2134.
44. K. Sun, Z. Xiao, S. Lu, W. Zajaczkowski, W. Pisula, E. Hanssen, J. M. White, R. M. Williamson, J. Subbiah, J. Ouyang, A. B. Holmes, W. W. H. Wong and D. J. Jones, *Nat. Commun.*, 2015, **6**, 6013.
45. X. Cheng, Z. Liang, S. Liang, X. Zhang, J. Xu, Y. Xu, W. Ni, M. Li and Y. Geng, *J. Mater. Chem. A*, 2023, **11**, 13984-13993.
46. L. Yang, J. Qin, S. Li, J. Zhang, Y. Yang, B. Cao, C. He and J. Hou, *Energy Fuels*, 2021, **35**, 19756-19764.
47. X. Zhu, B. Xia, K. Lu, H. Li, R. Zhou, J. Zhang, Y. Zhang, Z. Shuai and Z. Wei, *Chem. Mater.*, 2016, **28**, 943-950.
48. R. Sun, Y. Wu, J. Guo, Y. Wang, F. Qin, B. Shen, D. Li, T. Wang, Y. Li, Y. Zhou, G. Lu, Y. Li and J. Min, *Energy Environ. Sci.*, 2021, **14**, 3174-3183.
49. P. Yin, Y. Ma and Q. Zheng, *J. Mater. Chem. A*, 2022, **10**, 10400-10407.
50. J. Min, X. Jiao, V. Sgobba, B. Kan, T. Heumüller, S. Rechberger, E. Spiecker, D. M. Guldi, X. Wan, Y. Chen, H. Ade and C. J. Brabec, *Nano Energy*, 2016, **28**, 241-249.
51. M. J. Newman, E. M. Speller, J. Barbé, J. Luke, M. Li, Z. Li, Z.-K. Wang, S. M. Jain, J.-S. Kim, H. K. H. Lee and W. C. Tsoi, *Sci. Technol. Adv. Mater.*, 2018, **19**, 194-202.
52. S. Li, Q. Ma, B. Qiu, L. Meng, J. Zhang, Y. Wu, Z. Zhang, Z.-G. Zhang and Y. Li, *Solar RRL*, 2021, **5**, 2100515.
53. R. Cheacharoen, W. R. Mateker, Q. Zhang, B. Kan, D. Sarkisian, X. Liu, J. A.

Love, X. Wan, Y. Chen, T.-Q. Nguyen, G. C. Bazan and M. D. McGehee, *Sol. Energy Mater. Sol. Cells*, 2017, **161**, 368-376.

54. Y. Qin, N. Balar, Z. Peng, A. Gadisa, I. Angunawela, A. Bagui, S. Kashani, J. Hou and H. Ade, *Joule*, 2021, **5**, 2129-2147.

55. M. Ghasemi, N. Balar, Z. Peng, H. Hu, Y. Qin, T. Kim, J. J. Rech, M. Bidwell, W. Mask, I. McCulloch, W. You, A. Amassian, C. Risko, B. T. O'Connor and H. Ade, *Nat. Mater.*, 2021, **20**, 525-532.